Fan, Y., Rouholahnejad-Freund , E., Wagener, T., & al., E. (2019). Hillslope Hydrology in Global Change Research and Earth System Modeling. *Water Resources Research*, *55*(2), 1737-1772. https://doi.org/10.1029/2018WR023903

Structures and Functions of Hillslope Hydrology with Relevance to Earth System Modeling: Syntheses and Testable Hypotheses

Y Fan[1]*, M Clark[2], D M Lawrence[2], S Swenson[2], L E Band[3], S L Brantley[4], P D Brooks[5], W E Dietrich[6], A Flores[7], G Grant[8], J W Kirchner[9], D S Mackay[10], J J McDonnell[11], P C D Milly[12], P L Sullivan[13], C Tague[14], H Ajami[15], N Chaney[16], A Hartmann[17,21], P Hazenberg[18], J McNamara[7], J Pelletier[19], J Perket[2], E Rouholahnejad-Freund[20], T Wagener[21], X Zeng[18], E Beighley[22], J Buzan[23], M Huang[24], B Livneh[25], B P Mohanty[26], B Nijssen[27], M Safeeq[28], C Shen[29], W van Verseveld[30], J Volk[31], D Yamazaki[32]

1*. Corresponding Author; Dept of Earth and Planetary Sciences, Rutgers University, New Brunswick, NJ
2. National Center for Atmospheric Research, Boulder, CO
3. Department of Environmental Sciences, University of Virginia, Charlottesville, VA
4. Earth and Environmental Systems Institute / Dept of Geosciences, Penn State University, University Park, PA
5. Department of Geology & Geophysics, University of Utah, Salt Lake City, UT
6. Department of Earth and Planetary Science, University of California – Berkeley, Berkeley CA
7. Department of Geosciences, Boise State University, Boise, ID
8. College of Earth Ocean and Atmospheric Sciences, Oregon State University, Corvallis, OR
9. Department of Environmental Systems Science, ETH Zürich, Zürich, Switzerland
10. Department of Geography, The State University of New York at Buffalo, Buffalo NY
11. School of Environment and Sustainability, University of Saskatchewan, Saskatoon SK, Canada
12. U.S. Geological Survey, Princeton NJ
13. Department of Geography & Atmospheric Science, University of Kansas, Lawrence, KS
14. Bren School of Env. Science & Management, University of California – Santa Barbara, Santa Barbara, CA
15. Department of Environmental Sciences, University of California – Riverside, Riverside, CA
16. Department of Civil and Environmental Engineering, Duke University, Durham, NC
17. Department Earth and Environmental Sciences, Universities of Freiburg, Freiburg, Germany
18. Department of Hydrology & Atmospheric Sciences, University of Arizona, Tucson, AZ
19. Department of Geosciences, University of Arizona, Tucson, AZ
20. Laboratory of Hydrology and Water Management, Ghent University, Ghent, Belgium
21. Department of Civil Engineering, University of Bristol, Bristol, UK
22. Department of Civil and Environmental Engineering, Northeastern University, Boston, MA
23. Department of Earth, Atmospheric and Planetary Sciences, Purdue University, West Lafayette, IN
24. Atmospheric Sciences and Global Change Division, Pacific Northwest National Laboratory, Richland, WA
25. Department of Civil, Environmental & Architectural Engineering, University of Colorado - Boulder, Boulder CO
26. Department of Biological and Agricultural Engineering, Texas A&M University, College Station, TX
27. Department of Civil and Environmental Engineering, University of Washington, Seattle, WA
28. School of Engineering, UC at Merced, Merced, CA / USDA Forest Service, PSW Research Station, Fresno, CA
29. Department of Civil, Environmental Engineering, Pennsylvania State University, University Park, PA
30. Department of Catchment and Urban Hydrology, Deltares, Delft, The Netherlands
31. Department of Geological Sciences & Engineering, University of Nevada, Reno, NV
32. Institute of Industrial Science, The University of Tokyo, Tokyo Japan

Key Points

1. Lateral flow from ridges to valleys, and contrasts between sunny and shady slopes organize water, energy and vegetation across landscapes.
2. These processes may affect Earth System Model predictions of terrestrial water storage and fluxes, as well as ecosystem resilience to stress.
3. The greatest knowledge gap is the subsurface structure; Critical Zone science can offer new insights into terrestrial water storage/fluxes.

Descriptive Headings

Abstract

Earth System Models (ESMs) are essential tools for understanding and predicting global change, but they cannot explicitly resolve hillslope-scale terrain structures that fundamentally organize water, energy, and biogeochemical stores and fluxes at sub-grid scales. Here, we bring together hydrologists, Critical Zone scientists and ESM developers, to explore how hillslope structures may modulate ESM grid-level water, energy and biogeochemical fluxes. In contrast to the one-dimensional (1D), 2-3m deep, and free-draining soil hydrology in most ESM land models, we hypothesize that 3D, lateral ridge-to-valley flow through shallow and deep paths, and insolation contrasts between sunny and shady slopes, are the top two globally quantifiable organizers of water and energy (and vegetation) within an ESM grid cell. We hypothesize that these two processes are likely to impact ESM predictions where (and when) water and/or energy are limiting. We further hypothesize that, if implemented in ESM land models, these processes will increase simulated continental water storage and residence time, buffering terrestrial ecosystems against seasonal and interannual droughts. We explore efficient ways to capture these mechanisms in ESMs and identify critical knowledge gaps preventing us from scaling up hillslope to global processes. One such gap is our extremely limited knowledge of the subsurface, where water is stored (supporting vegetation) and released to stream baseflow (supporting aquatic ecosystems). We conclude with a set of organizing hypotheses, and a call for global syntheses activities and model experiments to assess the impact of hillslope hydrology on global change predictions.

1. Hydrology in Earth System Models

Earth System Models (ESMs) are essential tools for understanding and predicting global environmental change. They must simulate the multitude of interactions within and among the atmosphere, the land, and the oceans through physical, chemical and biogeochemical pathways. Designed for global coverage and century-long simulations of fast atmospheric motion, ESMs are built on large model grid cells (0.2^{o} - 2^{o} latitude-longitude, ~ 20km - 200km), which cannot explicitly resolve finer-scaled but fundamental processes in the atmosphere, the oceans, and the land alike. On land, as ESMs incorporate ecosystem and biogeochemical processes, their ability to predict terrestrial water stores and fluxes becomes increasingly important because of the ubiquitous role that water plays in regulating biogeochemistry and sustaining ecosystems and societies. As ESMs continue to move toward increasingly mechanistic process representation and increasing breadth of the processes that are represented, they will require their modeled hydrology to advance along with their other aspects. Many land model processes depend on the details of the hydrologic states, e.g., vegetation water stress and plant distribution, organic matter decomposition, methane production and emissions, fire ignition and spread, soil thermodynamics, nutrient leaching, dissolved organic and inorganic carbon export, and irrigation. In addition, as large-scale models begin to sharpen their focus on societally-relevant issues such as water and land management and water security, the importance of getting runoff and streamflow correct (for the right reasons) also grows.

Hydrologic processes are traditionally studied at hillslope-to-catchment scales (10s of meters to kilometers). At this scale, topographic gradients from ridges to valleys drive water, sediment and biogeochemical fluxes down the hillslopes and out of the catchments. And at this scale, the sunny and shady sides of a ridge exhibit contrasting radiative, hydrologic and ecological conditions. Field instruments are traditionally aligned with, and hillslope- and catchment-scale models are built to capture, such fundamental gradients across the landscape (e.g., Dunne and Black, 1970; Wilson and Dietrich, 1987; McDonnell, 1990; Band et al., 1991, 1993; Band, 1991, 1993; Duffy, 1996; Montgomery et al., 1997; Ebel et al.,2007; Hwang et al., 2009; McGuire and McDonnell, 2010; Nippgen et al., 2015; Bergstrom et al., 2016; Angermann et al., 2017; Staudinger et al., 2017). Recently, Critical Zone (CZ) science – the study of the structure, function and evolution of the soil and underlying regolith (the weathered mantle overlying fresh bedrock) that support terrestrial life (e.g. Brantley et al., 2006, 2017a) – has catalyzed an integrative, system-level approach toward understanding the co-evolution of the landscape and terrestrial life, bringing together diverse perspectives from the broader Earth Surface Processes community.

In this new CZ science, hillslopes and catchments remain as the scales of instrumentation, conceptualization, and modeling, for they continue to be recognized as fundamental organizers of water, energy and biogeochemical states and fluxes across the landscape (Brantley et al., 2017b; Rempe and Dietrich, 2018). Over the past six decades or so, hillslope and catchment research has produced prodigious field observations, theories and models, at individual research sites and across organized research networks including the LongTerm Ecological Research network and the USDA Agricultural Research Service and Forest Service experimental watersheds (e.g. Stringer et al., 2016). The nascent international network of Critical Zone Observatories (CZOs) is

laying the foundation for cross-site syntheses (e.g. Paola et al., 2006; Brantley et al., 2017a; Baatz et al., 2018), making possible a global assessment of the most salient structures and functions of hillslope processes that may matter to large-scale fluxes in ESMs. Thus catchment and CZ scientists, as a community, can offer deep insights into the lay of the land, and we hope to tap into their collective wisdom so that we can identify the most critical processes to implement in ESMs.

At the planetary scale, ESMs embody our best understanding of Earth system interactions, and the IPCC (Intergovernmental Panel on Climate Change) studies of past and future climate depend on ESMs. In the early years, hydrology was portrayed as one-dimensional (1D, vertical) infiltration into, and evapotranspiration (ET) from, the surficial soils, neglecting the 3D (vertical + lateral) water movement on and below the land surface. As ESMs include sub-grid terrestrial vegetation dynamics (e.g., Fisher et al., 2018) and human impacts such as large-scale irrigation (e.g., Leng et al., 2013), a land hydrology with comparable sub-grid complexity has become justifiable. In this synthesis, we bring together the hydrology-CZ community and the ESM community to achieve the following objectives: (1) to identify the sub-ESM-grid-scale processes that are fundamental organizers of hydrologic stores and fluxes across the landscape that may matter to ESMs, (2) to explore simple mechanistic ways to implement them in ESMs, and (3) to formulate a set of testable hypotheses and future global synthesis efforts to test them.

This synthesis builds onto an earlier paper by Clark et al. (2015) outlining challenges and opportunities for improving land hydrology in ESMs. Clark et al. (2015) articulated the scientific motivations and reviewed hydrologic process representations in current ESM land models. They highlighted the gaps between ESM hydrology and current process understanding in the hydrology and CZ communities, and identified key opportunities to advance ESM hydrology. These opportunities include (1) representing hillslope-scale lateral hydrologic convergence and two-way surface-groundwater exchange, (2) a comprehensive benchmarking system using hydrologic and CZ observations, and (3) stronger interactions between the CZ and ESM communities (exemplified by continental-scale hydrologic modelling uniting the hydrology and ESM communities; Archfield et al., 2015). Subsequent workshops and proof-of-concept testing using the Community Land Model (CLM) further shaped the discussions. These discussions converged on the need to (1) pool the diverse views in the hydrology and CZ community, (2) set priorities among the multitude of processes viewed as important, and (3) recommend to the ESM community what hydrologists and CZ scientists consider as the most salient structures and functions of sub-ESM-grid processes. Through CUAHSI (https://www.cuahsi.org/) we initiated a call for white paper contributions, followed by a series of webinars and meetings at the annual AGU (American Geophysical Union) conference. Here, we report the outcome of these discussions.

As reviewed in detail by Clark et al. (2015), early ESM land models described land hydrology as 1D fluxes, partitioning canopy throughfall into surface runoff versus infiltration, then partitioning infiltration into soil storage supporting ET versus deep drainage loss to river baseflow. In this 1D construct, a model grid cell was a large flat slab with no local topographic gradients, i.e., the hydrologic condition was uniform within a grid cell (~20-200 km

wide). This approach neglected certain processes that are important at the landscape scale – specifically, the lateral flow from ridges to valleys and the topographic controls on solar insolation. In addition, the large model slab was only a few meters thick and freely drained; drainage water was placed in the model "river storage" instantaneously, neglecting drainage impediment due to shallow water tables in lowland valleys, and the delayed discharge into streams via lateral flow in the subsurface. The consequence of this 1D free-draining model construct, e.g. in the Amazon, was fast drainage loss during wet periods (Miguez-Macho & Fan, 2012a), reduced terrestrial water storage in dry periods (Pokhrel et al., 2013), and shutting down of ET and headwater streamflow in the dry season (Miguez-Macho & Fan, 2012b), contrary to flux tower and streamflow observations.

The past decades have seen several advances in the representation of land hydrology in ESMs. One example is the use of the variable-source area concept (e.g., Hewlett and Hibbert, 1967; Dunne and Black, 1970) and the application of TOPMODEL (Beven and Kirkby, 1979) to divide large model cells into zones of varying saturation (more in Section 4), capturing localized surface-runoff production and the disproportionate impact of riparian transpiration (Famiglietti and Wood, 1994). The second example is the redistribution of snow based on terrain characteristics (e.g., Liston 2004) The third is treating individual grid cells as mosaics of different surface properties, such as land-use and cover types, further refined by dividing vegetated patches into plant functional types (PFTs), e.g. forests vs. grasslands (Koster and Suarez, 1992). However, the structures and functions of the terrain within a grid cell remained largely absent; there is no explicit and dynamic lateral flow from uplands to lowlands (except by Subin et al., 2014), nor are sunny and shady slopes distinguished from one another. The modeled distribution of PFTs (e.g. grassland vs. forest) is generally (with some exceptions, e.g., the ORCHIDEE Land Model, https://orchidee.ipsl.fr/about-orchidee/) not associated with local hydrologic conditions, even though these conditions vary systematically from uplands to lowlands and from sunny to shady slopes, which may explain the patchwork of different PFTs under any given climate. The common disassociation of PFTs from their water-energy environment makes it difficult for models to predict that forest ET can continue over part of the landscape, despite water-stressed conditions on average (Miguez-Macho and Fan, 2012b). At a fundamental level, topographic complexity alters the amount and timing of energy and plant-available water across the landscape. The resulting spatial variability in energy-water coupling is reflected in the covarying spatial structure of vegetation, soil and regolith development, biogeochemical fluxes, and other aspects of the CZ. Recent advances in the mechanistic understanding of these interactions call for a renewed evaluation of how to best represent land hydrology in ESMs.

From the perspective of hillslope and catchment hydrologists and CZ scientists, there are many aspects of ESM hydrology that are considered unrealistic and in need of major revisions or expansions (as reviewed in Clark et al., 2015). CZ science is revealing increasing complexities and evermore nuanced insights, particularly regarding moisture availability in the weathered bedrock beneath soil (Salve et al., 2012; Rempe and Dietrich, 2018), subsurface preferential flow paths with multiple perched lateral flows (the fill and spill concept; Tromp-van Meerveld and McDonnell, 2006), and the intermittent hydrologic connectivity that drives plant water use and

geochemical releases from catchments (e.g., Hopp and McDonnell, 2009; Lanni et al., 2011; Godsey et al., 2009; McDonnell, 2014; Brantley et al., 2017b; Rahman and Rosolem, 2017). Indeed, attempts have recently been made to represent the rapid recharge to the deep store via rock fractures in global models (Vrettas and Fung, 2015, 2017; Hartmann et al., 2015; 2017). However, the state of knowledge and the lack of global subsurface data do not yet allow us to test the importance of these emerging properties. And given the increasing complexity of ESMs and the associated computation burden, it is prudent to focus on the first-order and well-understood processes. For example, that water flows downhill, and that the sunny slopes are warmer and drier than shady slopes, have been long and universally acknowledged. Incorporating these processes in ESMs – through characterization and estimation of their grid-scale functions – may now be possible, given the global availability of hillslope-resolving topographic data. Therefore our focus will be on processes that are obvious and quantifiable, and that can potentially impact ESM predictions in water-stressed places and times.

These considerations will guide the presentation below. We seek to identify salient structures and processes that a) shape the abiotic and biotic landscape, b) have the potential to alter large-scale water, energy and biogeochemical fluxes between the land and the atmosphere, c) can be described by basic physical principles with a few measurable parameters, and d) can be tested by comparing model outcomes against observations. We pose the following questions to the two communities jointly.

(1) How does the terrain (topography, lithology, geomorphic history) organize the regolith (soil and weathered bedrock) and vegetation and the stores and fluxes of water, energy, and carbon across the landscape? (Section 2)

(2) How does this terrain influence vary throughout the world under the wide range of climate-terrain combinations? Where do we expect the greatest impact on ESM water, energy and carbon fluxes? (Section 3)

(3) How do we divide an ESM grid cell into functional units that best reflect terrain controls? How do we represent the connectivity among the units? And how do we parameterize the models from observable variables? (Section 4)

(4) What are the testable hypotheses regarding the terrain-driven CZ structures and functions in the context of ESM predictions and global change research? What are the immediate and future efforts needed to test these hypotheses? (Section 5)

The purpose of this synthesis is two-fold. On one hand, we strive to distill the best process understanding from the broader CZ community to improve ESM realism. ESMs are powerful tools for synthesizing and testing first-order Earth-system-level interactions, and they are the only tools for the society to foresee the future. The CZ community has the knowledge and hence the obligation to contribute to ESM advancement. On the other hand, as future ESMs become able to capture processes at scales meaningful to CZ scientists, the CZ community will gain a powerful tool to explore coupled climate-CZ co-evolution, the notion of a dynamic CZ regulated by, and regulating, global change (Gaillardet et al., 2018). Our emphasis here on connecting site-based science to global predictions resonates with the decades-long effort in the hydrology community to seek and organize hydrologic similarities

with the aim of predicting un-observed places (McDonnell and Woods, 2004; Wagener et al., 2007). The CZ-ESM collaboration can offer new motivation and momentum for ongoing inquiries, expose new knowledge gaps, and generate new hypotheses. Hence the intended audience of this paper includes both the broader hydrology and CZ community, who observe and decipher how nature works at the inherent scales, and ESM developers and users, who must abstract the first-order interactions to make global predictions.

We emphasize the impact of present-day terrain structure on land hydrology, neglecting hydrologic regulation of weathering and erosion that shape the landscape at geologic time scales. Although these long-term processes are a central focus of CZ science, the design time scales of ESMs (seasonal to decadal) dictate that we first assume a static landform, which controls the short-term dynamics of water storage and flow. However, to characterize the depth profile of soil/regolith permeability and porosity in hilly terrain – which are critical to water storage and flow but not directly observable – we must depend on CZ knowledge of the processes and geomorphic history that have created the landscape we see today. Therefore our synthesis will probe into the depth structure of the CZ along hillslope profiles, but will be limited to what they look like now, to help parameterize water storage and transmission in the model soil/regolith.

We focus on vegetation and its associated ET flux for the following reasons. First, natural vegetation selects, adapts to, exploits and thus expresses the integrated water-energy-nutrient environment. By observing vegetation, which is readily observable at individual, stand, ecosystem and global scales, one can infer the critical resources that are limiting (e.g., Meinzer, 1927). Secondly, vegetation exerts a strong influence on CZ evolution through myriad pathways (e.g., Roering et al., 2010; Sullivan et al., 2016; Brantley et al., 2017c); thus understanding landform-vegetation relations is a key CZ inquiry. Thirdly and critically, plant photosynthesis and ET are the primary pathways for land-atmosphere exchange of water, energy, and carbon, and hence understanding the structure and function of vegetation is of central interest to ESMs and global carbon cycle research.

2. Terrain Organization of Vegetation and ET via Water and Energy

It is well known that vegetation patterns follow the topography in mountainous terrain (e.g., von Humboldt, 1807; Schimper, 1903). Figure 1(b) reproduces the famous tableau of von Humboldt describing the vertical vegetation zones encountered on his ascent of the Andes in 1799-1803. The sheer elevation range, from sea level to over 4000m, gives rise to a steep climate gradient that underlies the striking vegetation gradient described by von Humboldt. The entire vertical range occurs within a horizontal distance of only ~1^{o} longitude (~100km at the equator), the dimension of a typical ESM grid cell (Figure 1c). Clearly, in such regions of the world, the many plant functional types within an ESM grid cell would have little meaning without their relation to the elevation range they occupy.

In flatter parts of the world (e.g. the central Amazon, Figure 1d), the elevation range and climate gradient are subdued. Local gradients dominate the relief, and a regular motif of plateaus, side slopes, and stream valleys ensues. The climate here does not exhibit striking vertical zones, and the local hydrologic gradient emerges as a

key differentiator for vegetation (e.g. Whittaker, 1956; Day and Monk, 1974; Hales et al., 2009; Schietti et al., 2014; Moulatlet et al., 2014; Hoylman et al., 2018).

As ESM land model grid cells approach a fraction of a degree (1/8-1/5°, or ~12.5-20km), the vertical climate zonation will further decrease. At the 20km grid scale (e.g., Figure 1e), it may be reasonable to neglect vertical climate zonation in moderate- to low-relief terrain, and to represent it in steep terrain through sub-grid atmospheric down-scaling. In the discussions below, we assume that the regional climate is uniform across an ESM grid cell, and under this uniform climate, we examine how the local terrain and hydrology may organize the vegetation. We focus on two basic hillslope structures: the gravity-driven down-valley convergence of surface and subsurface flow, and the systematic difference in insolation between sunny and shady slopes.

2.1. Down-Valley Drainage

Here the term drainage includes both the vertical percolation at any position on the landscape and the lateral, ridge-to-valley convergence of surface and groundwater, both driven by gravity. Hill-to-valley convergence creates drier hills and wetter valleys, resulting in deep or absent water tables under the hills, and shallow water tables under the valleys. This hill-to-valley convergence facilitates efficient vertical drainage in uplands and impedes drainage in valleys, thus forming riparian wetlands. In places and times with water stress, a wetter valley can support higher plant productivity than one would expect from the climate alone. Figure 2a shows a landscape in the southwestern United States under a semiarid climate. The valley-hill hydrologic contrast translates directly into a vegetation contrast. Here the plant functional types (aspen forest vs. desert shrub/grass), duly differentiated in ESMs, correlate well with drainage positions. Without this inherent coupling and assuming uniform soil water status across an ESM grid cell, it would be difficult to predict the continued transpiration from the aspen forest through the entire growing season. This ridge-to-valley subsidy also occurs in seasonally dry climates where abundant wet season precipitation recharges the regolith and groundwater (Goulden et al., 2012; Swetnam et al., 2017; Tai et al., 2017; Schwantes et al., 2018). Groundwater flow converges toward the valleys with a delay, and continues into the dry season, because groundwater moves slowly. Gallery forests line the stream corridors, such as in the Mediterranean climate of central California (Figure 2b) and the monsoonal climate of eastern Africa (Figure 2c). The latter landscape lies in a transition zone between rainforests and open savanna, which can coexist owing to the effects of topographic relief (Kim and Eltahir, 2004). In the landscapes represented by Figure 2a-c, it is aridity, at least seasonally, that makes hill-to-valley drainage relevant to vegetation patterns.

In humid and low-relief regions where water is in excess, lateral drainage is also important, but for different reasons. Here regional drainage is impeded, resulting in waterlogged soils and oxygen stress for plants. The slightly elevated hills can improve local drainage and alleviate waterlogging. In the vast seasonal wetlands of the Pantanal (Dubs, 1992) (Figure 2d), the low hills support islands of forests above the poorly drained grasslands. In the white-sand forests of Rio Negro in Venezuela (Figure 2e), the slightly elevated sandy hills are excessively drained and support low Bana forests only, while the lowlands are perennially waterlogged and support palms only, and the intermediate positions are occupied by high Caatinga forests (Coomes and Grubb, 1996). The mosaic

appearance of the boreal forest in northern Denmark (Figure 2f) reflects drainage, and in this cold region, drainage also affects soil temperature and growing season length, with waterlogged soils warming up later in the springtime. A positive feedback reinforces the terrain-vegetation association; denser vegetation and higher ET on higher terrain further lowers the water table, improving drainage and nutrient conditions and enabling higher productivity and higher ET, and so forth (Sullivan et al 2016). In the landscapes represented by Figure 2d-f, it is too much water, and the associated soil oxygen stress, that make lateral drainage important to vegetation patterns.

2.2. Slope Aspect Difference

Another widely acknowledged consequence of topographic relief is that it creates variations in local solar angle and thus the intensity of solar radiation received at the surface. In places and times with energy limitation, warmer slopes can support longer growing seasons. Conversely, in places and times with water stress, cooler slopes can support higher plant productivity. Figure 3 gives examples in the Northern Hemisphere (north toward the right in all images) where south-facing slopes are warmer and drier as articulated by the vegetation (e.g. Ping et al., 2005; Bennie et al., 2006; Newman et al., 2014; Brooks et al., 2015; Smith et al., 2017; and a synthesis by Pelletier et al., 2018). In arid western Texas (Figure 3a), and seasonally arid California (Figure 3b) and Idaho (Figure 3c), the cooler north-facing slopes support a moister habitat and mesic vegetation. At a site in Israel, north-facing slopes harbor higher vegetation biomass with lower susceptibility to insect herbivory (Auslandera et al., 2003). In regions that depend on winter snowpacks for warm-season water supply, snow persists longer into the summer on north-facing slopes (Figure 3d), delaying water release into the dry season. In landscapes represented by Figure 3a-d, it is aridity, at least seasonally, that makes topographic aspect relevant to vegetation patterns.

In the energy-limited high latitudes of the Yukon (Figure 3e), tree-line position and species richness and turnover are best explained by slope aspect, because soils thaw more deeply on the warmer south-facing slopes (Dearborn and Danby, 2017). That tree-line position and ecotonal plant community composition vary systematically across hillslope aspects is a long and well-established concept (e.g., Johnson, 1848; Elliott and Kipfmueller, 2010; Elliott and Cowell, 2015). Near Fairbanks, Alaska (Figure 3f), south-facing slopes with well-developed silt loam soils support mature white spruce that "should be rated among the most rapidly growing and valuable forest stands of interior Alaska" (Krause et al., 1959), while on the north-facing side of the ridge, "a poorly drained half-bog soil supports a stand of dwarfed black spruce with an extremely slow growth rate". Krause et al. (1959) also wrote that "none of the alterations of the vegetative cover is comparable to the radical and lasting changes imposed by micro-climatic influences on slopes of different exposures, especially those of northern and southern aspects." At such high latitudes, the low sun angle amplifies even low relief, affecting permafrost thawing, land drainage and aeration, and vegetation phenology (e.g., Ping et al., 2005; Endalamaw et al., 2017). In landscapes represented by Figure 3e-f, it is energy stress, at least seasonally, that makes topographic aspect relevant to vegetation patterns.

The generalizations presented above are complicated by the intersections between aspect-driven energy availability and gravity-driven lateral drainage. In warmer locations or on sunny slopes, valleys harbor greater

biomass (Swetnam et al., 2017; Perdrial et al., 2018), but in cooler locations and/or shady slopes, valleys support lower biomass (Zapata-Rios et al. 2016). In more mesic locations, the observed systematic increase in biomass downslope has been attributed to nutrient subsidies carried by the lateral hydrologic subsidy (Weintraub et al., 2017; Shi et al., 2018). By mechanistically representing these fundamental drivers and their interactions, ESMs can offer a powerful tool to elucidate the complex patterns of vegetation distribution across the globe.

2.3. Soil/Regolith Thickness along Topographic Gradients

A critical parameter in ESM land models is the so-called "soil depth", intended to include sufficient soil water storage to support ET during the dry intervals between precipitation events. Early models included the top 2m of the land surface, thought to represent the depth containing the bulk of the root biomass in woody plants (e.g., Sellers et al., 1996a, 1996b). Such model soil depths were found to be inadequate to explain the high dry-season ET in the Amazon, where deeply weathered tropical soils extend far deeper and roots were seen at 11m depth (Nepstad et al. 1994). ESM simulations of ET and regional climate are highly sensitive to soil depth in the Amazon and elsewhere (Milly and Dunne, 1994; Kleidon and Heimann, 2000; Baker et al., 2008; Harper et al., 2010; Markewitz et al., 2010; Mankin et al., 2017), yet it is a poorly constrained parameter. The choice has been somewhat ad hoc, depending on convention and influenced by conflicting reports of rooting depths of particular plants in particular places; the report of 11m deep roots by Nepstad et al. (1994), for example, motivated model studies with 10m soil depth (e.g., Baker et al., 2008; Lee et al., 2005). Yet the question remains: what is the right model "soil depth"? How deep is deep enough in different parts of the world? What is the scientific basis for defining model "soil depth", and how can it be quantified across the diverse environments of the world?

The struggle to define the right "soil depth" by ESM scientists in many ways parallels the struggle to define the thickness of the Critical Zone by CZ scientists (see a recent attempt by Riebe et al., 2017). Both communities have in mind the layer of Earth surface material that is porous and permeable, that envelops the circulation of meteoric water, that supports terrestrial life, and that is physically, chemically and biologically altered by water and life. In this regard, knowledge of CZ depth and structure, one of the central inquiries of CZ science, is directly relevant to clarifying, conceptualizing and quantifying the "soil depth" in ESMs.

Because of the difficulties in seeing the subsurface, our knowledge of the depth and structure of the CZ is very limited. Figure 4 offers a few "windows" into the dark belowground, showing cross-sections of the CZ along ridge-valley transects at several US CZOs, obtained from coring (Figure 4a, core locations given) and a variety of subsurface geophysical inversion tools, particularly seismic velocity that indicates rock density, degree of fracturing and/or porosity development. Some tentative, ESM-relevant remarks can be made across these sites, which are limited in sample size but cover a range of climates, lithologies, plant biomes and landforms, and thus can at least prompt some fruitful synthesis questions.

First, the porous/permeable and hydrologically active layer is far thicker than the 2-3m depth commonly assumed in ESM land models. At the Eel River CZO in California (Figure 4a, Rempe and Dietrich, 2018), the traditionally defined soil is only 0.5-0.75m thick, but the underlying weathered or fractured bedrock is also

hydrologically active, and is >20m thick. Roots were found in fractures at 16m depth tapping the "rock moisture" (exchangeable water stored in the unsaturated zone in the weathered bedrock), which held more than 1/4 of the annual precipitation, sustaining the Douglas fir forest through the dry summer. The "rock moisture" zone is also the primary conduit for lateral groundwater drainage from hills to valleys that sustains stream baseflow at this site. At the Southern Sierra CZO, also in California (Figure 4b, Holbrook et al., 2014), about one-third of annual ET comes from water storage below 1m depth in the deeper regolith; this storage is recharged during the winter and is available for tree use during the summer and fall (Bales et al., 2011; Klos et al., 2018). The importance of weathered and fractured rocks in supporting ET is widely recognized in mountainous terrain with a dry season (Arkley, 1981; Miller et al., 2010; Graham et al., 2010; Bales et al., 2011; Goulden et al., 2012; Salve et al., 2012; Rempe and Dietrich, 2018; Johnson et al., 2018). Thus in hilly terrain where the "soil" is shallow, and in biomes where plants depend on deep moisture in the dry season, ESM "soil depth" must include the weathered or fractured rocks to account for the observed dry-season plant survival.

Second, in general the vertical change in porosity/permeability with depth can be gradual, particularly in warmer and wetter environments where weathering fronts are deep (Figure 4f, lower two rows). This gradual change – in physical, chemical, and biological markers alike – makes defining the base of the CZ difficult (Riebe et al., 2017), particularly in areas of the world underlain by deep sediments with a deep, long-distance regional groundwater flow system (Schaller and Fan, 2009). From the hydrologic perspective, it is difficult to define the base of groundwater flow without deep profiles of material properties. Given that deeper processes are generally associated with longer time scales, and given that the slow processes can be important to ESM objectives (e.g., deeper flow sustains baseflow and riparian ecosystems in drought months and years), a sharp cutoff depth can be difficult to delineate across the wide range of hydrogeologic conditions of the world. Instead, an approach that quantifies the vertical gradients in subsurface properties may be more meaningful, as elaborated later in Section 4 on parameterizing the model lower boundary.

Third, there is evidence that the CZ thickness and structure may correlate with topography, which to a large extent drives water and sediment fluxes, and weathering and erosion rates that shape CZ thickness. Moving from the valley bottom to the ridge top, the porous-permeable layer thickens at the California sites (Figure 4a, b), but the shape of the fresh bedrock boundary differs (convex vs. concave up). Rempe and Dietrich (2014) propose that the vertical advance of the weathering front is controlled by the rate of drainage from the fresh bedrock, and they present an analytical model to predict the convex shape of the hilltop and the underlying transition to fresh bedrock, as well as the consequent upslope thickening of the weathered profile. At the Boulder Creek CZO in Colorado (Figure 4c, d for two sub-catchments), the soil/regolith is thicker under the valleys in the upper catchments (Figure 4c, sections 1 and 2; Figure 4d, section 1), because recent river incision has not reached this far upstream, and the present regolith profiles reflect a past climate (Befus et al., 2011). The cross-section at the Shale Hills CZO in Pennsylvania indicates no systematic trend (Figure 4e), although the latest data (not shown) indicate that the regolith is thicker under the ridgelines.

Figure 4f reveals the possible interplay between the local topography and the regional tectonic stress field in initiating CZ development. The high correlations among the rock failure potential (left column), the stress field (middle column), and the seismic velocity (right column, reflecting rock density) are striking across the three sites representing very different lithologies, climates and histories (Boulder Creek CZO in Colorado, Calhoun CZO in North Carolina, and Pond Branch in Maryland). These observations raise the possibility of predicting the CZ depth, or at least the hard-rock threshold, based on our knowledge of tectonic stress fields and the readily available high-resolution maps of surface topography (Slim et al., 2015; Riebe et al., 2017 and their Hypothesis 1).

Across hillslope aspects, there is a difference between south- and north-facing slopes at Boulder Creek CZO (Figure 4c, d), with substantially thicker soil and regolith on the north-facing slopes (left side of the figures). Stronger frost action is proposed as a key factor (Anderson et al., 2013; Riebe et al., 2017 and their Hypothesis 2). The weathered zone also seems thicker on the north-facing slope at Shale Hill CZO (Figure 4e) despite a steeper slope, which is suggested to reflect the relic periglacial landscape from the last ice age; a modeling study here suggests that ~100 mm more water passes annually through the north-facing than the south-facing slopes. At the Reynolds Creek CZO in southwestern Idaho, Geroy et al. (2011) wrote, "Soils on the north aspect retain as much as 25% more water at any given soil water pressure than samples from the south aspect slope. Soil porosity, soil organic matter and silt content were all greater on the north aspect, and each contributed to greater soil water retention. These results, along with the observation that soils on north-aspect slopes tend to be deeper, indicate that north-aspect slopes can store more water from the wet winter months into the dry summer in this region, an observation with potential implications on ecological function and landscape evolution." But in studies in the Yukon (Dearborn and Danby, 2017) and Alaska (Krause et al., 1959), the opposite seems true, with south-facing slopes supporting more deeply thawed, drained and developed soils, which in turn support larger vegetation and higher productivity. Thus it appears that, where water is most limiting, the north-facing slopes are hydrologically and ecologically more active, with water and life penetrating deeper into the substrate, both critical agents of weathering and CZ deepening, but where energy is most limiting, the south-facing slopes are hydrologically and ecologically more active. This is a hypothesis to be tested globally (Section 5).

The above discussions only touch upon a few of the many nodes and threads of an enormously complex system of process interactions that shapes the structure of the modern-day CZ. But they raise the possibility of simplification, extrapolation and global prediction, albeit crudely and tentatively. A key question is, what do we know now, that will allow us to improve upon the current ESM “soil depth” prescriptions?

2.4. Plant Rooting Depth along Drainage Gradients

The link between the moisture stored in the CZ and the aboveground vegetation is the plant root system. As the pioneer root ecologist Weaver (1919) stated, “one cannot understand why a particular plant is found in a particular place without knowing its root system”. Among the many root traits, the rooting depth is perhaps the closest proxy for the depth of the CZ that is exploited and altered by vegetation. Here we ask the question, are there systematic changes in plant rooting depth along drainage and aspect gradients? Because roots are difficult

to observe, we have only a very limited view of their morphologies and functions. Existing observations seem to suggest that hillslope hydrology is an important driver of plant rooting depth (Fan et al., 2017). Figure 5A plots 2020 rooting depth observations of >1000 species, on a log scale, against several abiotic and biotic factors. At a given mean annual precipitation (a), or within a given soil texture class (b), rooting depths vary over orders of magnitude. Although larger and evergreen plants (d) tend to develop deeper roots, rooting depths vary widely within individual growth forms. Of the 30 best-sampled genera, species in arid and semi-arid climates tend to develop deeper roots, but the wide range underscores the large plasticity of root response to local conditions.

These local conditions include bedrock depth (c) and water-table depth (f). The strong correlation with bedrock and hardpan depth (c) hints at the importance of knowing the CZ structure and physical barriers to root penetration. But more than half of the sampled roots penetrated below the barriers, either as a result of ambiguous reporting of bedrock depth, or as a testimony to plants' persistence in securing resources. Since water is a primary resource, the strong correlation with water-table depth (f) is unsurprising. As conceptualized in Figure 5B, the moisture profile at any location may vary systematically from the hill to the valley. The profile is wetted above by intermittent infiltration, and wetted below by steady capillary rise from the water table. In between there may exist a dry gap of varying duration, which narrows toward the valley. Roots of plants on the ridge (position 1) cannot cross the dry gap and are limited to shallow infiltration depths (Cannon, 1911; Bucci et al., 2009). At the lower position 2, roots may sense the capillary rise, and dimorphic roots develop, with a shallow cluster using rain and a deep cluster using groundwater in dry seasons (Howard, 1925; Kimber, 1974; Dawson and Pate, 1996). At position 3, infiltration meets capillary rise and water is not limiting. At position 4, seasonal waterlogging limits roots to the oxygenated soils above the water table, and shallow or aerial roots are common in lowland forests (Smith, 1972; Stone and Kalisz, 1991; Pavlis and Jenik, 2000). At position 5, permanent waterlogging selects wetland species that are insensitive to the water table.

These observations provide evidence that plant rooting depths co-vary with CZ structure and hydrology, and that the aboveground organization of vegetation by hillslope hydrology is facilitated by belowground root-water relations. These relations are the biophysical link between CZ hydrology and land plants. By resolving the fundamental gradients in CZ hydrology (including soil moisture, rock moisture, and the water-table depth) across the landscape, ESM land models can avoid prescribing plant rooting depth, and instead let the CZ moisture profile and plant water demand dictate the necessary depth of root growth (Fan et al., 2017).

3. Global Significance of Terrain Influence on Vegetation

The above highlights of the well-known terrain influence on vegetation through drainage and aspect, and the less well-known terrain influence on soil/regolith depth and structure (which in turn determine the water storage capacity for ET), are based on anecdotal, location-specific evidence (Figure 1-4). The next questions are: where and when, across the diverse and dynamic environments of the globe, do we expect that these terrain influences will matter to ESM predictions of large-scale water, energy and biogeochemical fluxes? Do such areas

494 add up to a significant portion of the global land area? And will the hillslope-scale structures, however
495 deterministic and predictable, simply average out over an ESM grid cell and hence matter little to global
496 predictions?

497 Regions of strong topographic relief are obvious candidates for strong terrain influence, but strong relief
498 is unnecessary under some conditions and insufficient under others. For example, if an ESM grid cell with strong
499 relief is located in the ever-wet tropics, with no water or energy limitations on photosynthesis, then down-valley
500 drainage will have little impact on either uplands or lowlands, both receiving abundant and frequent rain to sustain
501 ET, and both well drained to maintain aerated soils. Its tropical latitude will minimize the aspect difference as well.
502 Thus, topographic relief will be most important under certain combinations of climate and terrain that create
503 water shortage or waterlogging, or energy stress. Figure 6 illustrates some of the end member climate-terrain
504 combinations where (a) down-valley drainage and (b) aspect difference may matter. The example of the ever-wet
505 tropics with high local relief (assuming no substantial climate zonation) would map onto position 1 in Figure 6a.

506 As postulated in Figure 6a, down-valley drainage may matter the most in a seasonally dry climate with
507 moderate to high relief (position-4 and 5). Examples are Figure 2b and c. The wet season ensures water surplus in
508 part of the year, and the relief drives upland surplus toward the lowlands. Depending on slope length and gradient,
509 the flow will take time, so that the spatial carry-over from uplands to lowlands implies a temporal carry-over from
510 wet to dry seasons, supplying ET in lowlands and dry seasons. In such places, although the portion of the landscape
511 (or grid cell) remaining green in the dry season may be small, the continued survival of valley forests may have far-
512 reaching ecological and societal consequences. Although a similar argument can be made regarding positions 7
513 and 8 (arid climate) in Figure 6a, without a strong wet season there is little surplus for spatial-temporal carry-over
514 and the importance of down-valley drainage is diminished. However, a wetter riparian corridor can exist further
515 down the regional gradient along larger rivers fed by long-distance groundwater convergence, discussed further in
516 Section 4 on regional-scale hydrologic connectivity.

517 Down-valley convergence also matters in sites under ever-wet climate with low relief (position 3, Figure
518 6a). Here the problem is too much water, and the elevated mounds improve local drainage and support higher
519 productivity. Examples are Figures 2e and f. The same occurs in a climate with seasonal flooding (position 6, e.g.
520 Figure 2d). If captured in ESMs, the improved drainage of the low hills can support islands of larger vegetation that
521 would otherwise be impossible.

522 As shown in Figure 6b, aspect variations are highest in the high latitudes, especially in moderate- to high-
523 relief landforms (positions 1 to 2), which are found to be the strongest factors driving plant distribution (Dearborn
524 and Danby, 2017, Figure 3e; Krause et al., 1959, Figure 3f). At the high latitudes, even low relief (position 3) can be
525 amplified by the low sun angle. Such predictable variations in insolation, if captured in ESMs, will result in longer
526 snow-ice and soil-groundwater residence times in the shady portion of the landscape, affecting the period of
527 snowmelt, permafrost freeze/thaw, vegetation phenology and ET.

Figure 6 suggests that terrain influence on vegetation matters the most where vegetation is under stress (e.g., in water, energy, or soil oxygen), at least seasonally. Such places often mark the transitions of biomes, or ecotones, where terrain-driven local variations in the stressors may create different plant habitats. The position of the tree-line is an example; the tree-line elevation and the associated transitional plant community composition are markedly different on south vs north-facing slopes (Johnson, 1848; Krause et al., 1959; Elliott and Kipfmueller, 2010; Elliott and Cowell, 2015; Dearborn and Danby, 2017). Another example is the forest-savanna transition marked by increasing seasonal drought; here the valleys support forests and hills support grasslands (Cole, 1992; Furley, 1992; Thompson et al., 1992; Ratter, 1992; Dubs, 1992; Grogan and Galvão, 2006; Jirka et al., 2007; Bucci et al., 2008; Villalobos-Vega, 2010; Rossatto et al., 2012). All the examples in Figures 2 and 3 are places where water or energy is limiting (too little or too much). This is a hypothesis to be tested as discussed in Section 5.

To assess the global extent of terrain influence (do they add up to a substantial area of the land surface?), we may outline and exclude areas where it matters little (positions 1 and 9 in Figure 6a, and positions 6 to 9 in Figure 6b), as attempted in Figure 7b. Regarding drainage, position 1 (ever wet, high relief, well-watered and well-drained) is excluded in turquoise (Af climate in Figure 7a). Position 9 (arid climate, low relief) is excluded in red. It can be hypothesized that over the rest of the world, lateral drainage may differentiate hydrologic and plant conditions within an ESM grid cell. Regarding aspect, positions 7 to 9 in Figure 6b (tropical latitudes) are excluded in orange, and position 6 (mid-latitude, low relief) in yellow. It can be hypothesized that over the rest of the world, slope aspects may differentiate energy, water and plant conditions within a grid cell. This qualitative assessment suggests that over the majority of the land surface, drainage and aspect potentially play a role in creating systematic and predictable variations in water and energy states, leading to systematic and predictable variations in ecosystem types and functions within an ESM grid cell. This is a hypothesis to be tested as discussed in Section 5.

A key question is how these sub-grid structures affect grid-mean states and fluxes communicated to the atmosphere in ESMs; i.e., do the sub-grid variation average out over a grid cell? The answer requires quantitative analyses accounting for the non-linear processes linking water and energy availability to ET fluxes. Such an attempt was recently made by Rouholahnejad-Freund and Kirchner (2017). They assessed the impact of sub-grid heterogeneity and lateral drainage on grid-mean ET, based on the Budyko model (Turc, 1954; Mezentsev, 1955) of mean annual ET as a non-linear function of mean annual precipitation (P) and potential evapotranspiration (PET). Since P and PET (input variables) vary spatially across an ESM grid cell, there are two ways to compute the spatially averaged ET (output): averaging the input or averaging the output. The difference, termed the “heterogeneity bias”, turned out to be always positive, i.e. ET is always over-estimated by averaging the heterogeneous climatic inputs rather than averaging the heterogeneous outputs (which is what the real-world atmosphere does, at the scale of ESM grid cells). This finding is relevant to the aspect effect discussed above, whereby PET can vary substantially within an ESM grid cell on sunny vs. shady slopes. Most ET models include substantial non-linearities and will similarly lead to “heterogeneity bias”, although different models may lead to either over- or under-estimates, depending on whether the non-linearity is downward- or upward-curving. Rouholahnejad-Freund and

Kirchner (2017) also assessed the effect of lateral drainage by adding upland surplus (P-PET) onto lowland P. They found that grid cell average ET is enhanced only where the upland has a surplus and the lowland has a deficit. However, the annual-mean Budyko model does not include seasonal variations in P and PET and the storage from wet to dry seasons, so the significance of the down-valley drainage is probably under-estimated. Further global analyses and modeling that resolve seasonal and inter-annual storage dynamics are urgently needed, as discussed in Section 5 on testable hypotheses and future tasks.

4. Representing Hillslope Hydrology in ESMs

Here we address the following questions. How should we divide a 20-200km wide ESM grid cell into functional units that best reflect our understanding of terrain control on vegetation dynamics? How should we represent the connectivity among these units? And how should we parameterize the models based on physical principles and globally available observations? We explore how to represent the hydrologic structures and functions with conceptual clarity and parametric and computational efficiency. ESMs cannot and need not resolve every hillslope, but can succinctly capture the effects of ridge-valley gradients and sunny-shady exposures.

We define a hillslope as the strip of land connecting a ridge line to its nearest stream in the valley (e.g., at the scales in Figures 2-4). Because ridges and valleys can be defined at nested scales (e.g., Montgomery and Dietrich, 1988) and because wetted channel networks are dynamic (e.g., Marani et al., 2001; Godsey and Kirchner, 2014), an inherent scale ambiguity is unavoidable. But for practical purposes, the degree to which a ridge and a stream can be resolved depends on the resolution of the digital terrain data, globally available at 1 arc-second (~30m) grids. In the discussions below, we assume that this grid resolution is sufficient to reveal the main terrain and vegetation structures within an ESM grid cell. We also assume that, with ESM grid scales approaching 20km in the near future, the vertical climate zones can be neglected in characterizing land hydrology, but can be captured as fine-scaled atmospheric forcing via atmospheric downscaling in steep terrain.

4.1. Subdividing an ESM Grid Cell into Hydrologic Functional Units

Implicit and equilibrium hydrologic partitioning

As reviewed in Clark et al. (2015), many attempts have been made to represent landscape heterogeneity within large ESM grid cells, from deterministic differentiation to statistical characterization of varying land surface properties. One particularly relevant effort is the application of TOPMODEL (Beven and Kirkby, 1979) toward partitioning a grid cell into drainage units. TOPMODEL uses a digital elevation model (DEM) to derive a topographic wetness index (TWI), the ratio of the logarithm of the contributing area above a unit contour length to the local terrain slope, reflecting a balance between topographic convergence (inflow) and local drainage (outflow). A map of TWI across a catchment, with high values in convergent and low-gradient valleys, and low values on divergent and high-gradient hilltops, elegantly and powerfully captures the essence of topography-driven hillslope and catchment hydrology. A large ESM grid cell can be partitioned into TWI zones, reflecting varying likelihoods of

water deficit or excess, with infiltration and ET calculated on each zone separately. Various TOPMODEL-based approaches have been implemented in large-scale models (e.g. Famiglietti and Wood, 1994; Koster et al., 2000; Walko et al., 2000; Niu et al., 2005; Clark and Gedney, 2008) as reviewed in detail by Clark et al. (2015). What is missing in this approach is the explicit and dynamic treatment of surface and groundwater convergence (Beven, 1997; Beven and Freer, 2001). TWI is applied instantaneously to redistribute the grid-cell water balance across the zones. Doing so assumes that hydrologic equilibrium is achieved within a model time step (minutes in ESMs), without explicit calculations of the variable flow rates from ridges to valleys, the intermittent connectivity between them, and the delayed delivery from uplands to lowlands.

Explicit and dynamic hydrologic partitioning

Several approaches have been used to partition large model grid cells into distinct drainage zones and to explicitly and dynamically route the flow down the gradient (see review in Clark et al., 2015). One simple approach is to divide an ESM grid cell into elevation bands (e.g., Nijssen et al., 1997). Over each band, standard 1D (vertical) fluxes are computed, and the surplus is routed from high to low bands, both above and belowground. This approach has the ability to represent vertical climate zones in high-relief terrain, and it is particularly useful for modeling snow dynamics (see review by Clark et al., 2011). Because each elevation band contains both hillslope and channel elements, this approach requires tracking both hillslope and channel dynamics within each band, as well as routing surface water and groundwater among the bands. An approach that separates hillslope and channel processes can improve the conceptual clarity and computational efficiency.

This can be achieved by using the concept of "equivalent" or "representative" hillslopes (Hazenberg et al., 2015; Ajami et al., 2016), where hillslope and channel processes are treated separately. Using high-resolution DEMs, channels are defined first, and the hillslopes are delineated by connecting channels to ridgelines. The numerous and complex hillslope forms in an ESM grid cell are collapsed into a few theoretical hillslope types, such as convergent, uniform and divergent slopes (Fan and Bras, 1998) and convex vs concave (in plan or profile) forms (Troch et al., 2003), and headwater vs side slopes (Hazenberg et al., 2015; Ajami et al., 2016). Each representative hillslope type consists of multiple "columns" of varying widths and elevations, along which water is routed from high to low columns, and only the lowest column feeds into the streams. This approach separates hillslope processes from channel processes, and the theoretical abstractions allow analytical insights (Troch et al., 2003), but in practice it can be difficult to reduce the highly complex terrain into a few theoretical hillslope forms.

Recognizing this challenge, Chaney et al. (2018) introduced a statistical approach to group the hillslopes into natural clusters. Within an ESM grid cell, along the channel network, hillslopes are traced upward, each with attributes including geometry, aspect, soil and vegetation. A cluster analysis is then used to reduce the large number of computed hillslopes into a (user-specified) number of characteristic forms. In doing so, many of the co-varying features of the landscape are implicitly considered in grouping the hillslopes (see also Flügel, 1995; Newman et al., 2014). These characteristic hillslopes have been represented in ESMs implicitly (Milly et al., 2014) and explicitly (Subin et al., 2014, Chaney et al., 2018). In the explicit approach, the characteristic hillslopes are

discretized into multiple height bands above nearest drainage, each band further sub-divided into different land cover-soil types.

Recently, the concept of HAND (Height Above Nearest Drainage), first proposed by Nobre et al. (2011), has emerged as a powerful way to divide an ESM grid cell into distinct drainage zones according to the drainage position of each DEM pixel along the ridge-valley transect. The DEM elevation of a pixel is referenced to the global mean sea level (Figure 8a, an example in central Amazon), whereas the HAND value of the pixel is the elevation referenced to its nearest stream channel following surface flow directions (Figure 8b), thereby removing the regional topography and retaining only hillslope-scale topography. All stream pixels in a grid box have a HAND value of zero, although they occur at different elevations. The next HAND level represents the riparian zone immediately above and surrounding the streams, and so forth. Figure 8c shows a histogram of the HAND values from Figure 8b, which separates, without overlap, the distinct drainage zones in the grid box. In the central Amazon, these distinct positions are related to the water-table depth (Figure 8d) and hence HAND can substitute for water-table depth as a powerful delineator of plant community composition and species turnover, also shown in Figure 8d (Schietti et al., 2014).

In the context of this discussion, HAND offers a simple way to divide an ESM grid cell into zones with linear drainage relations, so that the higher HAND zone drains only into the successively lower zone via hillslope flow, and only the lowest zone interacts with the streams. An example is shown in Figure 8e, where a watershed is divided into five HAND zones modeled as five steps (Figure 8f), each with its own elevation and lateral distance above the stream, its own surface area, and its own contact width with the adjacent zones. This approach is similar to the representative hillslope concepts above, but without fitting the complex terrain into a set of hillslope types. Instead, a watershed or grid cell is represented by a single (giant) slope which can be very wide, and the area of the zones adds up to the total grid cell area, facilitating water and energy budget closure. Hillslope aspect calculations can be readily performed at the DEM pixel level, and each HAND band can be further segregated into multiple aspects, similar to a stadium with tiers of seats facing different directions. HAND has been used to map continental-scale flood inundation (Zheng et al., 2018; Liu et al., 2018) and it is increasingly employed as an ecosystem niche indicator (Schietti et al., 2014; Moulatlet et al., 2014). Global high-resolution DEM data has been processed to derive HAND values (Yamazaki, 2017) which can be readily applied.

4.2. The Depth and Nature of the Lower Boundary

ESMs need to specify the model "soil depth" and the hydrologic conditions at this depth. Here we explore how to constrain this variable across the globe based on our knowledge of the depth-structure of the CZ and globally available information such as climate, tectonic stress, lithology, topography, soil, and vegetation.

Past ESM land models, with their 1D (vertical) construct, sought to represent the water storage in the plant rooting zone, assumed to be ~2m for woody plants and ~1m for herbaceous plants (e.g., Sellers et al., 1996a, 1996b). It was further assumed that soil drains freely, constrained by the hydraulic conductivity at the water content at the base of the soil column. Agricultural soil surveys provided particle-size information to compute

hydraulic properties via pedo-transfer functions (e.g., Clapp and Hornberger, 1978; van Genuchten, 1980; although these functions, based on mid-latitude soils, cannot represent the deeply weathered tropical clay which "holds on to moisture like clay but drains like sand" (Tomasella et al., 2000)). Such shallow and freely drained model soil columns have been shown to hold insufficient storage for continued ET in the dry season in the Amazon and other regions of the world with a strongly seasonal climate (e.g., Nepstad et al., 1994; Kleidon and Heimann, 1998; Baker et l., 2008; Miguez-Macho and Fan, 2012b; Milly and Shmakin, 2002; Brunke et al. 2016; Kuppel et al., 2017; Fan et al., 2017), prompting several inverse-modeling studies to estimate the "effective" root-zone depth necessary to support satellite-observed leaf area, based on seasonal precipitation and atmospheric ET demand (e.g. Kleidon and Heimann, 1998; Wang-Erlandsson et al., 2016; Yang et al., 2016; Fan et al., 2017). These inverse estimates place integrated (atmosphere, vegetation, soil) plant water constraints on the necessary model soil depth, but the persisting assumption that the land drains freely requires unrealistically deep soil column where the water table is within the 2-3m soil column and plant rooting depth is restricted by the shallow water table (Figure 5), such as in wetlands and river valleys. Such estimated deep soil column certainly meets ET demand, but it requires large carbon allocation toward root growth, biasing ESM carbon budget calculations.

As we advance ESM land hydrology beyond the 1D construct, and as ESMs attempt to represent groundwater and river dynamics and the ecosystems they support, the depth sufficient for ET may not be sufficient to encompass the zone of lateral groundwater flow that sustains stream baseflow and regulates regional aquifer systems. The zone of significant flow can occur below the rooting depth in the uplands, especially in the tropics where it can be tens to hundreds of meters deep (Ollier and Pain, 1996). Buss et al. (2013) report fractured flow at least 37m deep in the volcanic terrain at the Luquillo CZO in Puerto Rico, and 20m below the local stream, exporting water out of the catchment through the subsurface flowpaths that bypass local stream outlets. On the windward side of a volcano in Hawaii, Goodfellow et al. (2014) report weathering of basalts to >40m depth. This depth is even greater in large sedimentary basins that host the major aquifer systems of the world, such as the High Plains in the US where groundwater is recharged from the streams draining the Rockies hundreds of kilometers away, and where the aquifers supply the vast irrigated agriculture that fills the nation's "breadbasket" (Weeks et al., 1988; Winter et al., 1998). It seems that knowledge of the depth of significant porosity and permeability, or, equivalently, the depth of the CZ, is the most meaningful way to constrain ESM "soil depth".

The depth to the fresh bedrock has been estimated globally (e.g., Pelletier et al., 2016; Xu and Liu, 2017; Hengl et al., 2017) integrating various observations and models. These products for the first time offer a terrain-based, vs. the earlier climate plus biomass-based, global estimate of the depth to negligible fluid storage and motion, and thus an immediately useful product to constrain ESM soil depth. However, there remains the conceptual difficulty of drawing a physical line, above which there is fluid circulation and below which there is not. While this may occur in landscapes underlain by fresh bedrock, the transition from the high porosity/permeability surficial materials to the "tighter" deeper materials (mostly due to compaction in sedimentary basins) is usually fuzzy and transitional (Figure 4b, c, d, and f). This is more than a point of view; it also has physical implications. The

decrease in porosity and permeability with depth results in stratified groundwater flow rates and residence times, generally faster near the surface and slower at increasing depths. The slow deep flow imparts temporal persistence to the deeper moisture and baseflow to streams. In places with strong dry seasons and inter-annual droughts, it is the deep flow, which may be tens of meters deep, that delivers the water surplus from prior wet months and years to maintain valley groundwater and streamflow in dry months and years (Hodnett et al., 1997a, b; Ogden et al., 2013). In particular, this deep long-distance groundwater flow is the main source for streams and wetlands in arid regions (e.g., Schaller and Fan, 2009; Jobbagy et al., 2011), harboring ecosystem refugia with disproportionate ecological importance in an otherwise hostile and barren landscape (Fan, 2015; McLaughlin et al., 2017). Therefore, where deep hydrologic memory is needed to support ecosystems through droughts, it is necessary to account for the stratified flow system that results from the gradual reduction in porosity-permeability with depth. Thus instead of framing the problem as one of a definitive depth, it may be useful to frame it as one of a change in permeability and porosity with depth, with a characteristic vertical scale.

In general, porosity and permeability of continental crusts decrease with depth, and over depths of kilometers, the decrease appears linear in competent rocks such as sandstone and exponential in less competent rocks such as shale and mudstone (e.g., Manning and Ingebritsen, 1999; Shmonov et al., 2003; Saar and Manga, 2004; Stober, 2011; Kuang and Jiao, 2014). At depths of meters to tens of meters that are more relevant to ESM time scales, it is widely observed and modeled that porosity and permeability decrease exponentially with depth (Beven and Kirkby, 1979; Heimsath et al., 1997; Decharme et al., 2006; Cardenas and Jiang, 2010; Jiang et al., 2009, 2010; Wang et al., 2011; Sakata and Ikeda, 2013; Fan et al., 2013; Milly et al., 2014). An exponential function with monotonic decrease with depth does not represent the sharp transitions or local reversals in porosity and permeability that are frequently found in sedimentary rocks, but it preserves the overall trend while integrating fluid flow over depth, circumventing the difficult problem of parameterizing fine-scaled vertical heterogeneity. The exponential function also has other advantages. It represents the stratified flow system and preserves its dynamics across a range of temporal scales. By doing so, it also captures the negative feedbacks between the hydraulic head and the flow rate, whereby the lower head shifts the zone of flow to deeper and slower paths. This further reduces flow rate, contributing to the commonly observed long tails in streamflow recession curves (Eltahir and Yeh, 1999), and to the wide range of temporal scaling observed in chemical and isotopic tracers (Kirchner et al., 2001; Kirchner and Neal, 2013; Jasechko et al., 2016). Practically, it reduces model sensitivity to the choice of soil/regolith depth, and it allows for analytical integration of groundwater flow as a 2D problem, reducing computation and storage given the large demands on both in global ESM simulations.

If the problem is framed as one of change with depth, then our knowledge of lithology, topography, soil, vegetation and climate history can be used to constrain the rate of decrease, or the e-folding depth in the case of the exponential function. Given that hillslope-resolving topography is readily available globally, the e-folding depth has been formulated as a function of terrain slope (Fan et al., 2013), because the steepness of the land directly influences infiltration and weathering that thicken the CZ, versus surface runoff and erosion that thin the CZ

(Gilbert, 1909; Hooke, 2000). This approach was adopted in recent continental-scale studies (e.g. Maxwell and Condon, 2016; Gleeson et al., 2016; Zhang et al., 2016; Martinez et al., 2016). Going forward, multiple terrain attributes need to be considered besides steepness (e.g. Tesfa et al., 2009). Given the fundamental importance of rock lithology (e.g. Lebeveda and Brantley, 2017; Bazilevskaya et al., 2015), tectonic stress (e.g. St Clair et al., 2015), uplift and erosion rates (e.g. Rempe and Dietrich, 2014), the climate (e.g. Goodfellow et al., 2014; Anderson et al., 2013), climate history (e.g. Buss et al., 2013), and vegetation (e.g. Roering et al., 2010; Brantley et al., 2017c) as controls on CZ structure, a comprehensive approach considering these factors is needed. A useful question is whether existing global estimates of CZ depth, e.g. Pelletier et al. (2016) and Xu and Liu (2017), can inform global estimates of how porosity/permeability change with depth.

4.3. Lateral Hydrologic Connectivity within an ESM Grid Cell

Lateral flow from high to low drainage zones

By dividing an ESM grid cell into distinct drainage zones (e.g., Figure 8f), a traditional 1D soil hydrology model can be applied over each zone first, and the surplus, at each time step, can be routed down the drainage gradient toward the channel along surface and subsurface paths. The simplest way to compute lateral flow along a hillslope is the kinematic wave approximation, where the terrain slope substitutes for surface-water slope for routing surface runoff and streamflow, and for water-table slope for driving lateral groundwater flow. Beven (1981) reviewed the validity of this approach for groundwater flow, suggesting that it is best used in steep terrain with shallow bedrock where a perched water table nearly parallels the land surface. For global modeling representing the full range of hydrologic settings, the kinematic wave method must be used with caution.

Darcy's law is a fundamental physical law describing fluid flow in porous media driven by the hydraulic potential. Darcy's law has the same physical foundation as Ohm's law of electric currents driven by electric potentials, Dalton's law of evaporation driven by vapor pressure differences, and Fick's law of heat conduction driven by thermal gradients and molecular diffusion driven by concentration gradients. In Darcy's law, because the flow rate depends on the head, and the resulting head depends on the flow rate, a negative feedback ensues that accelerates drainage at times of high water tables and decelerates drainage at times of low water tables, leading to the characteristic asymptotic relaxation of the water table following a recharge pulse. Together with the decrease in porosity and permeability with depth, this negative feedback further prolongs deep soil water storage and hill-to-valley transfer into the dry season.

This negative feedback cannot be achieved with the kinematic wave approximation where the driving force (terrain slope) remains constant regardless of the water-table slope. Because the land is always steeper than the water-table slope, particularly in drier regions, using the land slope to drive flow depletes the water storage too soon, undermining a critical aspect of hill-to-valley delivery: the slow and delayed release of groundwater during the dry season. As the water table is explicitly tracked in some ESM land models (e.g., CLM), Darcy's law can be readily applied. With an exponential decrease in porosity-permeability downward, Darcy flow can be integrated analytically (e.g., Beven and Kirkby, 1979; Fan et al., 2007a), efficiently capturing both negative feedbacks.

Hillslope-channel exchange

The exchange between groundwater and streams can proceed in both directions (Winter et al., 1998). As illustrated in Figure 9a, across the hydrologic landscape from continental divides to the coastal oceans, a river can lose its water to the sediments or rock fractures below (Figure 9b, losing stream), or gain from the higher water table at the foot of the hillslopes (Figure 9c, gaining stream), all depending on the stream-groundwater level difference. This gradient can alternate in space along the same stream, such as from headwaters to lower reaches, and can also alternate in time, such as from rainy to dry periods. To represent this dynamic exchange across space and time, it is necessary to formulate the problem as potential-driven flow described by Darcy's law, as in the U.S. Geological Survey's MODFLOW model (Harbaugh et al., 2000). The barrier to the exchange, termed river hydraulic conductance, depends on the surface-groundwater contact area (river width x length in a grid cell, neglecting depth) and the riverbed permeability, all observable quantities, albeit poorly quantified over large areas.

Two additional feedback mechanisms are captured by the MODFLOW approach through the hydraulic barrier (river hydraulic conductance). First, riparian groundwater cannot instantaneously discharge to streams, limiting groundwater loss and prolonging the supply. Second, it is well known that, in humid climates, the stream channel network expands as the water table rises and intercepts a larger land area (higher river conductance), and contracts as it falls (e.g., Eltahir and Yeh, 1999; Marani et al., 2001; Jencso et al., 2009; Godsey and Kirchner, 2014). In dry and seasonally dry climates, this may be expressed as dry stream reaches (shorter active channels) in dry seasons and drought years (Lovill et al., 2018). The longer/wider streams accelerate groundwater discharge when the water table is high, and as the water table falls, the network shrinks and decelerates groundwater discharge, preserving storage and prolonging the recession. All of these self-regulating mechanistic "valves" in groundwater-surface water exchange act as delay mechanisms, so that the wet-season surplus stays in the system longer than it would otherwise.

In the lower floodplains of large rivers, an important mode of groundwater-river exchange is floodwater infiltration into bank and floodplain sediments, illustrated in Figure 9d. At stage A, the river is gaining, but at stages B and C, it is losing and filling bank and floodplain sediments. This bank and floodplain storage dampens peak flow and releases stored water to rivers and floodplain lakes long after the passing of flood waves. Floodplain storage and delay has been documented in the Amazon (e.g., Lesack, 1995; Lesack and Melack, 1995; Cullmann et al., 2006; Bonnet et al., 2008; Borma et al., 2009; Richey et al., 2011; Miguez-Macho and Fan, 2012a) where up to 30% of the river flow is estimated to have passed through the floodplain (Richey et al., 1989a, b). In drier climates with a deeper water table and larger water-storage capacity in the unsaturated sediments, river leakage is the primary groundwater recharge, as documented in the largest inland floodplains in Africa. For example, in the Okavango, 80–90% of the seasonal floodwater infiltrates, recharging groundwater and sustaining vast and vibrant wetland ecosystems in an arid climate (e.g., McCarthy, 2006; Bauer et al., 2006). In the Sudd, where the Nile River tops its banks annually, flooding raises the groundwater as evidenced by the large seasonal cycle in water-table depth with little local rainfall (e.g., Mohamed et al., 2006).

807 The above modes of groundwater - surface water exchange can be readily captured in ESMs via Darcy's
808 law (the MODFLOW approach) without user decisions and parameter-tuning, such as calibrating a "delay
809 parameter" in moving groundwater to rivers (e.g. Decharme et al., 2010). Using Darcy's law for surface water -
810 groundwater exchange without parameter tuning, Pokhrel et al. (2013) demonstrate that seasonal water storage
811 in the Amazon is closer to GRACE water storage change estimates, with peaks shifting later and wet-season storage
812 lasting longer, compared to the free-draining and one-way, instant placement of soil drainage into the rivers. The
813 groundwater-to-river delay varies in space and time and across scales. It is a natural outcome of potential-driven
814 flow operating under dynamic head gradient and resistance, which no single parameter can fully encompass.

815 ## 4.4. Lateral Hydrologic Connectivity among ESM Grid Cells

816 Aboveground, river flow is routinely routed among grid cells in ESM land models following river flow
817 directions. In most of these models, as the river passes through a grid cell it collects the drainage loss from the 1D
818 and freely drained model soil column, but it does not lose water to the grid cell. As discussed above, river leakage
819 loss to the sediment is known to support the vast and seasonally dynamic wetland ecosystems in inland basins
820 such as the Okavango, the Sudd, and the Pantanal, and it is a large term in the river water budget in these settings.
821 Thus allowing leakage loss is equally important to allowing seepage gain as the rivers pass through a grid cell.
822 River leakage loss in the headwaters (Figure 9e) also drives a deeper groundwater circulation. Stream bed
823 infiltration reaches the water table and flows toward regional discharge zones along deeper and longer paths,
824 resurfacing at larger channels down gradient, which tend to lie below the regional water table (Shen et al., 2016).
825 As illustrated in Figure 9f, groundwater flow can occur at multiple scales (Toth, 1963), with shallow and short "local
826 flow" to local streams, deeper and longer "intermediate flow" to higher-order streams down gradient, and even
827 deeper and longer "regional flow" to remote discharge zones such as coastal wetlands (Figure 9g). The impact of
828 the deeper flow on the basin water budget varies greatly, from >90% of local P-ET that leaves the basin through
829 the subsurface path (exporting groundwater) at one end, to streamflow eight-folds greater than its local P-ET
830 (importing groundwater) on the other, among the 1,555 US basins analyzed by Schaller and Fan (2009). This long-
831 distance groundwater transfer to down-gradient ecosystems, termed regional groundwater subsidy (Jobbagy et al.,
832 2011), is particularly important in drier landscapes (Figure 9e, lower panel); here the headwater streams lose
833 water to the regional water table, and that water only resurfaces at the lowest end of the regional gradient. Deep
834 and long-distance groundwater flow can also be important in humid landscapes that favor deep weathering;
835 Genereux et al. (2002, 2005, 2006) report significant inter-catchment groundwater transfer in the humid lowland
836 forests of Costa Rica, and Buss et al. (2013) report deep fractured flow 20m below local stream beds at the Luquillo
837 CZO in Puerto Rico, stating that "not all the water in the watershed is discharged to the stream."
838 The importance of groundwater flow among grid cells is a function of scale (Krakauer et al., 2014); larger
839 basins are more self-contained, with nearly all P-ET that leaves the basin passing the river outlet, but small low-
840 order streams collect only the shallow flows, with a large portion of the water budget leaving the catchment via
841 deeper paths bypassing the streams. For example, these deep flow paths are estimated to be 88% of the annual

budget of a 13km^2 forested catchment in southern Amazon (Neu et al., 2011). As ESMs adopt finer grids, the significance of among-grid-cell groundwater flow will increase. It is not difficult to calculate this flux given the mean water table of the grid cells. This flux is likely to be slow because it occurs in the deeper, less permeable rocks and sediments. But it is steady, reflecting and regulating the long-term dynamics of storage at interannual, decadal, or century scales. Spatially, this long-distance groundwater flow connects headwater losing streams with lower-reach gaining streams (Figure 9e), facilitating water budget closure within and among ESM grid cells.

Groundwater discharged at the lower end of long regional gradients is responsible for the belt of freshwater wetlands along the Atlantic and Gulf coasts (Figure 9g), fed by countless springs of aged groundwater (reviewed in Schaller and Fan, 2009; Fan and Miguez-Macho, 2011). Groundwater emerges before reaching the coastline because the sea level is the ultimate baseline for continental drainage. As the sea level fell more than 100m at the last glacial maximum, coastal wetlands moved offshore on the exposed continental shelves, and as the sea level rose, groundwater was backed up and wetlands moved inland (Faure et al., 2002). If ESMs are to predict, instead of prescribing, the major wetlands of the world, then long-distance groundwater flow among grid cells, ultimately tied to the global sea-level, would be a key mechanism necessary to predict the spatial distribution and temporal dynamics of wetlands in response to major shifts in the Earth's climate system.

4.5. A Land-Based Land-Model Grid System

The discussions so far conformed to the standard rectangular atmospheric grids of ESMs. Surface and shallow subsurface drainage are organized by a hierarchy of hydrologic units (hillslopes, low-order catchments, higher-order basins), and subsurface flow is controlled by the geologic and sediment structures. Neither conform to the Cartesian coordinates convenient for mathematical manipulation. In the earlier 1D land model construct, this fact hardly matters. But as we begin to recast the problem into 2D or 3D and account for lateral flow and deep flow, it would be natural to adopt a land-based grid system. Unlike the atmosphere and the oceans, landscape structures are permanent over ESM time scales, making them a natural framework for defining land grids.

Aboveground, a "grid cell" can be a catchment of certain ordered streams, which is self-contained in surface and shallow subsurface convergence, facilitating mass balance closure and correct flow routing among the "grid cells". With rectangular grids, a point near the edge of a grid cell may drain into the neighbor cell, or the stream in one cell can collect runoff from hillslopes in neighbor cells, a problem alleviated by using catchments as grid units. Catchment delineation is available globally (e.g., Lehner and Grill, 2013; Verdin, 2017), and this idea has been applied in several large-scale models (e.g., Koster et al., 2000; Goteti et al., 2008; Yamazaki et al., 2009, 2011; Beighley et al., 2009, 2011), in which the land-atmosphere flux exchange is computed on overlapping areas of the two grid systems. Besides conceptual and computation clarity, a catchment-based grid system will also yield ESM simulations of hydrologic conditions that are readily testable using the large number of streamflow observations around the world. The results will also be more meaningful to water resource managers whose jurisdictions are often defined by watershed boundaries.

Belowground, the water-table gradient sets the fluid in motion, but the flow path can be distorted by the geologic structure (e.g., Fan et al., 2007b; Meerveld and Weiler, 2008; Bense et al., 2013; Rempe and Dietrich, 2014; Hartmann, 2016). Groundwater basins are often incongruent with river basins (e.g., Schaller and Fan, 2009), and topography alone offers incomplete guidance, particularly in karst terrain (Ford and Williams, 2007; Worthington et al., 2016) where the cave and conduit network can reach >500 km (e.g., the Mammoth Cave System in Kentucky; Groves and Meiman, 2005) through which groundwater moves as fast as rivers. Recent work including karstic structures significantly altered the modeled hydrologic partitioning (Hartmann et al., 2015, 2017; Longenecker et al., 2017; Rahman and Rosolem, 2017). The karst example illustrates that many of the improvements in large-scale models would be futile without acknowledging such first-order geologic controls on groundwater flow. Global lithologic maps differentiating geologic provinces and rock types (Hartmann and Moosdorf, 2012), with detailed karst maps (Chen et al., 2017), and global estimates of permeability based on rock types (Gleeson et al., 2014; Huscroft et al., 2018) already exist. It is a logical step to "overlay" the geologic units onto the surface drainage units to jointly define a land-based land grid system that acknowledges the natural hydrologic plumbing network above and below the land surface.

5. Conclusions and Testable Hypotheses

In this synthesis paper, we attempted to answer the following questions: (1) What are the first-order structures and functions of hydrologic processes that organize water and energy across the landscape? (2) Where in the world do these structures and functions matter, and do they manifest themselves over large ESM grid cells, or do they simply average out? (3) How can we efficiently represent these structures and functions in ESMs, so that we can begin to test their large-scale significance? (4) What are the testable hypotheses regarding CZ structures and functions in the context of ESM predictions and global change research?

Regarding question (1), we conclude that among the myriad hydrologic processes across the wide spectrum of spatial-temporal scales, two terrain-induced hydrologic structures – the lateral drainage from hills to valleys, and the aspect difference between sunny and shady slopes – are first-order controls on water and energy availability across the landscape. Regarding question (3), the implicit "representative hillslope" concept and the application of potential-driven flow formulations can allow us to capture these first-order hillslope structures and the mechanistic feedbacks that regulate seasonal to decadal-scale dynamics.

However, regarding question (2), we do not yet know the answer. Our knowledge of hillslope and catchment hydrology leads us to hypothesize that, in water and energy limited places and times, hillslope-scale organization of water and energy can make a difference in ESM predictions. Below, we outline two sets of testable hypotheses in order to address questions (2) and (4). The first set will need to be tested through cross-network and cross-site synthesis efforts on the part of the hydrology, ecology and CZ science communities, and the second set to be tested through regional and global ESM modeling experiments.

H1. Ridge-to-valley drainage gradient and slope aspect difference are first-order organizers of CZ depth structure, water storage and flux, and vegetation across the landscape, under given climatic, lithologic and tectonic regimes and histories. To guide focused synthesis activities, we expand this hypothesis into the following.

H1a. The depth and the porosity-permeability structure of the Critical Zone, and thus the capacity for water storage and transmission, vary systematically from ridges to valleys and from sunny to shady slopes. The lack of a global view of CZ structure along drainage and aspect gradients remains the largest knowledge gap, which translates to large uncertainties in the capacity of the land to store and transmit water. Greater investment into "seeing" the subsurface, and cross-network and cross-site syntheses are needed to provide the ESM community with critical guidance on how to parameterize ESM model soil depth and properties.

H1b. In regions with seasonal water shortage, a greater valley storage can support larger plants, higher productivity and greater water use, and the hill-valley vegetation contrast is particularly pronounced during the dry season. An expression of this contrast is the mosaic of vegetation in the transition from tropical forest to savanna, with trees in valleys and grassland on ridges. The main hydrologic mechanism is down-valley lateral flow whereby upland surplus subsidizes lowland deficit (spatial carry-over). Slow subsurface flow delays the delivery to valley ecosystems, arriving long after rain or snowmelt events (temporal carry-over). Through such carry-overs, drainage positions organize plant available water and physiological water-use traits across space and time. A second mechanism for higher valley water availability is the larger water storage capacity due to thicker soils and sediments in valleys, in some places of the world, which is yet to be confirmed by testing H1a above.

H1c. In lowland areas with water excess (waterlogging), better-drained hills support larger plants and higher productivity. Two feedback mechanisms further enhance the plant-drainage association: high productivity and water use lowers the water table, further improving drainage; in cold regions, better-drained hills warm up earlier and use water earlier, further improving drainage and soil thermal status.

H1d. In regions with at least seasonal water shortage, shady slopes support larger plant forms and higher biomass, and the vegetation contrast across hillslope aspects is particularly sharp in the dry season (as grasses and herbs enter dormancy, and as trees restrict water use by stomatal and root response). The transition between forests and grasslands in water-limited mid-latitudes takes the form of a mosaic, with trees on shady slopes and grasslands on sunny slopes. A key hydrologic mechanism is the lower insolation and thus lower ET demand on shady slopes, reducing hydraulic failure and plant mortality. Another key mechanism is the higher water supply on shady slopes, due to their deeper soils and regolith which have greater water holding capacity, which is yet to be confirmed by testing H1a above.

H1e. In energy-limited regions, sunny slopes are warmer and support larger PFTs, and the contrast is particularly sharp at the beginning and the end of the growing season. The altitude of the tree-line varies accordingly (higher on sunny slopes and lower on shady slopes). In the high latitudes, aspect differences are amplified by the low sun angle, and the latitude of the transition between taiga and tundra vegetation varies accordingly. One mechanism is the longer growing day and growing season on sunny slopes. But another

mechanism is in the subsurface: the thicker soil and regolith development, and thus the thicker thawed and drained depth, on sunny slopes, which is yet to be confirmed by testing H1a above.

To test Hypothesis 1 above, cross-network and cross-site syntheses on current understanding of process controls on soil and regolith depth (for example, Pelletier et al., 2018) are needed. Such syntheses efforts, on where-how-which processes interact to create the modern-day CZ structure, will provide the core knowledge to extrapolate across the globe, utilizing globally available information on topography, uplift rates, tectonic stress fields (e.g., Heidbach et al., 2016), bedrock geology, climate, vegetation, and other relevant factors. Field observational campaigns are needed to map the CZ structure at endmember places and to test theories of CZ evolution. Such global extrapolation is necessary for constraining ESM soil depth and parameters that are critically important to water storage and flow, and thus to vegetation dynamics. Such an activity is synergetic with, and can reinvigorate, past hydrologic synthesis efforts to translate knowledge from observed to un-observed sites (e.g. Blöschl, 2006; Wagener et al., 2010). But here we call for more emphasis to be given to "seeing" the dark subsurface, which is difficult to observe but holds the key to understanding nearly everything we observe above the ground concerning the spatial structure and temporal dynamics of water and plants.

In addition, to test Hypothesis 1, global-scale, high-resolution and joint terrain, climate and vegetation analyses are needed. Global coverage and hillslope-resolving terrain data exist already, and global high-resolution vegetation data from satellites are available at seasonal to decadal time scales. A comprehensive mapping of vegetation distribution with regard to drainage position (as shown in Figure 2) and slope aspect (Figure 3), under different end-member combinations of terrain and climate of the world (as shown in Figure 6), can now be readily performed, which can provide an unprecedented global perspective on the explanatory power of terrain structure on vegetation distribution.

H2. Implementing hillslope drainage and aspect effects will alter ESM predictions of water, energy and biogeochemical fluxes from the land to the atmosphere in resource-limited places and times, through several direct and indirect mechanisms expanded below.

H2a. In water-limited regions, larger PFTs are associated with topographic valleys and shady hillslope aspects. In lowland regions with waterlogging and oxygen stress, larger PFTs are associated with topographic highs. In energy-limited regions, larger PFTs are associated with sunny hillslope aspects. By linking PFTs with the drainage and aspect they occupy, ESM land models will likely simulate higher plant productivity across the landscape, and the productivity is likely to be less sensitive to water and energy limitations. This is particularly so in places with seasonal water or energy limitations, because the favorable seasons will allow large growth and resource needs to be met in the stressed seasons.

H2b. By implementing ridge-to-valley groundwater convergence, which takes days to months, instead of instant drainage (as in the early 1D land models), and by allowing snow and rain to stay on the shady slopes longer, the net effect will be the lengthened residence times of precipitation on land. Except for the ever-wet places of the world, this implies greater water availability for vegetation in the dry intervals between precipitation or melt

events. Where water is limiting to vegetation, this implies higher ET flux to the atmosphere, and lower river runoff to the oceans.

H2c. The temporal delay inherent in the hill-to-valley delivery is accentuated by several "self-preserving" mechanisms. By using Darcy's law, by allowing stratified and deep flow (vs. a sharp cutoff depth), and by allowing two-way surface-groundwater exchange driven by the hydraulic potential and regulated by a dynamic river-groundwater connectivity, ESM land models will have longer hydrologic memory and persistence, to the benefit of the vegetation and aquatic ecosystems in water stressed seasons.

H2d. By extending model "soil depth" to include the weathered bedrock, informed by the knowledge of CZ structure, ESM land models will simulate a larger terrestrial water storage capacity, higher amplitude of seasonal and interannual change as seen by the GRACE satellite, and longer residence times of water on land. The deeper "model soil", and a better articulated hillslope hydrology, will allow the extension of plant rooting depth to respond spatially and dynamically to deeper moisture, further modulating plant distribution and ET along hillslope hydrologic gradients.

H2e. By differentiating uplands from lowlands and sunny from shady slopes, energy fluxes to the atmosphere can also be altered through changes in surface albedo due to changes in vegetation, even if the grid-mean latent heat flux is unaltered. The positive albedo feedbacks associated with snow further enhances snow persistence on shady slopes.

H2f. Wetlands are fundamentally land drainage features, and poor drainage occurs in all climates. By accounting for lateral flow within an ESM grid cell, ESM land models can mechanistically predict the location and dynamics of local wetlands. By allowing leakage loss from large rivers and long-distance groundwater flow among ESM grid cells that is ultimately linked to the sea level, ESM land models can mechanistically predict large regional wetlands.

H2g. A land-based land grid system, defined by catchments for surface and shallow subsurface connectivity, and geologic structures for deeper subsurface connectivity, offers conceptual and computational advantages. Such a system will render the hydrology in ESM land models more efficient, accurate, and testable at the grid cell level (catchments) with widely available streamflow observations. It will also make ESM predictions more useful for water resource managers.

H2h. By differentiating uplands from lowlands and sunny from shady slopes within an ESM grid cell, output from ESMs can deliver internally consistent, hillslope-scale hydrologic and ecosystem forecasts under future global change. This will expand the power and reach of IPCC future assessments to directly inform local policies and management decisions, bypassing the step of impact analyses through climate downscaling using different methods and assumptions.

To test Hypothesis 2 above, model experiments are needed to quantify the sensitivities of ESM simulations to the inclusion of hillslope hydrology. High-resolution, regional to continental-scale, off-line and coupled land-atmosphere model simulations have played a critical role in revealing how the finer hydrologic

structures can impact soil moisture, ET, wetland distribution, and land-atmosphere fluxes and regional climate (e.g., Maxwell et al., 2007; Maxwell and Kollet 2008; Miguez-Macho and Fan 2012a, 2012b). They will continue to play a critical role in testing some of the hypotheses posed above. However, these high-resolution models are still far from resolving the hillslope-scale structures emphasized here, there are no comparable high-resolution datasets to support them (Beven and Cloke, 2012), and they are computationally demanding and hence not yet feasible to be directly implemented in global and fully coupled ESM simulations. Therefore model experiments directly using ESMs are necessary. These experiments can involve a hierarchy of simulations of increasing complexity in terms of how the hillslopes are represented, how covariations of PFTs with topography are represented, and complexity of represented processed (e.g., carbon cycle, ecosystem demography). Additional experiments can include land-only versus coupled as well as transient historical simulations into the future. A systematic series of ESM "sensitivity" experiments, adding one hillslope structure, and one covariation in soil-regolith and PFTs at a time, will be useful toward testing each of the sub-hypothesis posed above. We hold the view that a new generation of land hydrology models that represent the fundamental scales and processes, and that are consistent in complexity and scale with the next generation of vegetation models tracking PFTs and the demographic structures within them (Fisher et al 2018), have the potential to elevate ESMs to a new level of realism in predicting ecosystem responses and feedbacks to global change.

More than ever, we are aware of humanity's power in shaping the future trajectory of this planet (Steffen et al., 2018). More than ever, we appreciate the residence and flow of fresh water on land for sustaining human societies and the natural systems on which humans depend. More than ever, we recognize the intricate linkages and feedbacks between the biotic and abiotic worlds, nearly all enabled by the common currency of flowing water. And more than ever, we have the necessity to foresee the future, via Earth System Models, so that actions can be taken to steer the planet on a sustainable path. With the dawn of a new century in AGU science and service to society, we link two communities across scales in the Earth Science, to translate what is learned from intensely measured field sites into Earth-System-Level interactions that shape the trajectory of this planet.

Acknowledgements

This community synthesis project is supported by the National Science Foundation directly through an INSPIRE grant (NSF-EAR-1528298) and indirectly through CUAHSI cooperative agreement (NSF-EAR-0753521). We thank the CUAHSI leadership (Rick Hooper and Jerad Bales) and staff, and NCAR leadership for their support, and the many members of the hydrology, CZ, and ESM community who contributed to the discussions at the workshops and webinars. Finally we thank Elenore Blythe, Dennis Lettenmaier, Keith Lucey, and two anonymous reviewers for their constructive comments which substantially improved the manuscript. There are no new data or models in this study.

Figure Captions

Figure 1. (a) Topography of the Amazon basin, (b) von Humboldt's (1807) famous tableau of vertical vegetation zones, (c) the topography of an area representative of von Humboldt's illustration, (d) topography near Reserva Ducke, and (e) a 0.2o window in a region in (d). The areas in (c) and (d) are 1x1o latitude-longitude windows with 0.2o (~20km) grid lines.

Figure 2. Contrasts in hydrologic conditions between hilltops and valleys as expressed by vegetation, in (a) water-stressed environment of Arizona (https://en.wikipedia.org/wiki/Desert_riparian), (b) summer-dry Mediterranean climate in central California (GoogleEarth), (c) Forest-savanna transition in Luama Katanga Reserve of eastern Congo (photo by Andrew Plumptre/WCS, https://news.mongabay.com/2014/11/mapping-mistake-leaves-wildlife-at-risk/), (d) seasonally water-logged (oxygen-stressed) Pantanal where larger vegetation occupies better-drained mounds (http://wikimapia.org/8582923/Pantanal-Mato-Grossense-National-Park), (e) white-sand community in lowland Venezuela with both excessive drainage of the sand and waterlogging (Terborgh 1992), and (f) the cool-wet lowlands of Denmark (Lille Vildmose Natural Park, https://en.wikipedia.org/wiki/Lille_Vildmose). The images span climatic gradients from hot and dry in (a) to cold and wet in (f), and high to low relief.

Figure 3. Contrasting energy-water-vegetation conditions between northern and southern exposure (north to the right in all images), in (a) water-limited environment of Texas (Guadalupe Peak in Guadalupe Mountains National Park, http://thecommonmilkweed.blogspot.com/2009/10/guadalupe-peak-hike.html), (b) seasonally water-limited California (GoogleEarth) and (c) southwest Idaho near Anderson Ranch Reservoir (https://upload.wikimedia.org/wikipedia/commons/d/d8/Effects_of_aspect_on_vegetation-_SW_Idaho.JPG). (d) Higher up in Idaho near Mount Cramer (GoogleEarth), snow persists into the summer on north-facing slopes. In energy-limited environments, (e) tree-line elevation and plant community composition differ across hillslope aspects in southwest Yukon (photo by Ryan Danby, Queen's University, Canada; used with permission) and (f) interior Alaska near Fairbanks (GoogleEarth).

Figure 4. Example cross-sections showing soil/regolith thickness and structure along hillslope transects at several US CZOs: (a) rock moisture and seasonal water table in the weathered bedrock at Eel River CZO (Rempe and Dietrich, 2018), (b) total water storage capacity (top) and interpreted porosity (ϕ) from seismic surveys at Southern Sierra CZO (Holbrook et al., 2014), (c)-(d) seismic velocity (a function of rock density and thus porosity) across several transects at Boulder Creek CZO (Befus et al., 2011), (e) seismic velocity at Shale Hills CZO (used by permission from S Brantley at SSHCZO), and (f) failure potential (left), compressional stress (causing fracturing) (middle) and seismic velocity (right) at Boulder Creek CZO (top), Calhoun CZO (middle), and Pond Branch (bottom) (St. Clair et al., 2015).

Figure 5. (A) Observed rooting depth (log-scale) vs. (a) annual precipitation, (b) soil texture class, (c) hardpan/bedrock depth, (d) growth form, (e) genera, and (f) water-table depth. (B) Schematic subsurface moisture profile along a drainage gradient, wetted from above by intermittent infiltration, and from below by steady capillary rise, with a dry gap that narrows downslope. Adapting to this gradient, plant rooting depths can vary systematically from the ridge to the valley (modified from Fan et al., 2017).

Figure 6. Schematic diagram of climate-terrain combinations where down-valley drainage (a) and difference in slope aspect exposure to the sun (b) can potentially influence ESM grid-level energy/water/carbon fluxes.

Figure 7. (a) World climate (from https://en.wikipedia.org/wiki/K%C3%B6ppen_climate_classification), and (b) world topography, with areas outlined where sub-grid topography will have minimal impact on local water and energy states and fluxes.

Figure 8. (a) Elevation above mean sea level in the Cuieiras catchment, central Amazon, (b) height above nearest drainage (HAND) over the same area, (c) frequency of HAND values for waterlogged, ecotone and upland vegetation (all from Nobre et al., 2011), (d) schematic of a HAND profile in Reserva Ducke where plant composition changes with HAND and depth to water table (Schietti et al., 2014), (e) an example to illustrate HAND bins above a channel (light blue line) in a catchment in Idaho, and (f) the HAND bins represented in models of four zones with different elevation, area, and interface width.

Figure 9. (a) Hydrologic landscapes from continental divide to coastal ocean, showing modes of surface-groundwater exchange: (b) losing streams, (c) gaining streams, (d) flooding and floodplain storage, (e) losing streams in headwater catchments feed regional groundwater flow toward gaining streams down gradient, which is more important in arid climate (Fan 2015), (f) Toth's theory of multi-scale groundwater flow (Schaller and Fan 2009) where lower and larger streams (right) receive regional groundwater (and river) convergence (R = recharge, Qr = river discharge, Qg = groundwater discharge bypassing nearest stream), and (g) US wetlands. Images (a) to (d) and (g) are from Winter et al. (1998).

References:

Ajami, H., U. Khan, N. K. Tuteja, and A. Sharma (2016), Development of a computationally efficient semi-distributed hydrologic modeling application for soil moisture, lateral flow and runoff simulation, Environ. Modell. Softw., 85, 319-331, doi:http://dx.doi.org/10.1016/j.envsoft.2016.09.002.

Anderson, R. S., S. P. Anderson, and G. E. Tucker (2013), Rock damage and regolith transport by frost: an example of climate modulation of the geomorphology of the critical zone, Earth Surface Processes and Landforms, 38(3), 299-316.

Angermann, L., C. Jackisch, N. Allroggen, M. Sprenger, E. Zehe, J. Tronicke, M. Weiler, and T. Blume (2017), Form and function in hillslope hydrology: characterization of subsurface flow based on response observations, Hydrol. Earth Syst. Sci., 21(7), 3727-3748.

Archfield, et al. (2015), Accelerating advances in continental domain hydrologic modeling, Water Resour. Res., 51(12), 10078-10091, doi:10.1002/2015WR017498.

Arkley, R. J. (1981), Soil Moisture Use by Mixed Conifer Forest in a Summer-Dry Climate, Soil Science Society of America Journal , 45(2), 423-42.7

Auslander, M., E. Nevo, and M. Inbar (2003), The effects of slope orientation on plant growth, developmental instability and susceptibility to herbivores, Journal of Arid Environments, 55(3), 405-416.

Baatz, R., et al. (2018), Steering operational synergies in terrestrial observation networks: opportunity for advancing Earth system dynamics modelling, Earth Syst Dynam, 9(2), 593-609, https://doi.org/10.5194/esd-9-593-2018.

Baker, I. T., L. Prihodko, A. S. Denning, M. Goulden, S. Miller, and H. R. da Rocha (2008), Seasonal drought stress in the Amazon: Reconciling models and observations, J Geophys Res-Biogeo, 113, G00B01, doi:10.1029/2007JG000644.

Bales, R. C., J. W. Hopmans, A. T. O'Geen, M. Meadows, P. C. Hartsough, P. Kirchner, C. T. Hunsaker, and D. Beaudette (2011), Soil Moisture Response to Snowmelt and Rainfall in a Sierra Nevada Mixed-Conifer Forest, Vadose Zone J, 10(3), 786-799, DOI: 10.2136/vzj2011.0001.

Band, L. E. (1991), Distributed Parameterization of Complex Terrain, Surv Geophys, 12(1-3), 249-270.

Band, L. E., D. L. Peterson, S. W. Running, J. Coughlan, R. Lammers, J. Dungan, and R. Nemani (1991), Forest ecosystem processes at the watershed scale: basis for distributed simulation, Ecological Modelling, 56, 171-196.

Band, L. E. (1993), Effect of land surface representation on forest water and carbon budgets, Journal of Hydrology, 150(2), 749-772.

Band, L. E., P. Patterson, R. Nemani, and S. W. Running (1993), Forest ecosystem processes at the watershed scale: incorporating hillslope hydrology, Agricultural and Forest Meteorology, 63(1), 93-126.

Bauer, P., T. Gumbricht, and W. J. W. R. R. Kinzelbach (2006), A regional coupled surface water/groundwater model of the Okavango Delta, Botswana, Water Resour. Res., 42(4), W04403, doi:10.1029/2005WR004234.

Bazilevskaya, E., G. Rother, D. F. R. Mildner, M. Pavich, D. Cole, M. P. Bhatt, L. X. Jin, C. I. Steefel, and S. L. Brantley (2015), How Oxidation and Dissolution in Diabase and Granite Control Porosity during Weathering, Soil Sci Soc Am J, 79(5), 55-73, doi:10.2136/sssaj2014.04.0135.

Befus, K. M., A. F. Sheehan, M. Leopold, S. P. Anderson, and R. S. Anderson (2011), Seismic Constraints on Critical Zone Architecture, Boulder Creek Watershed, Front Range, Colorado, Vadose Zone J, 10(3), 915-927.

Beighley, R. E., K. G. Eggert, T. Dunne, Y. He, V. Gummadi, and K. L. Verdin (2009), Simulating hydrologic and hydraulic processes throughout the Amazon River Basin, Hydrol Process, 23(8), 1221-1235, http://dx.doi.org/10.1002/hyp.7252.

Beighley, R. E., R. L. Ray, Y. He, H. Lee, L. Schaller, K. M. Andreadis, M. Durand, D. E. Alsdorf, and C. K. Shum (2011), Comparing satellite derived precipitation datasets using the Hillslope River Routing (HRR) model in the Congo River Basin, Hydrol Process, 25(20), 3216-3229, http://dx.doi.org/10.1002/hyp.8045/.

Bennie, J., M. O. Hill, R. Baxter, and B. Huntley (2006), Influence of slope and aspect on long-term vegetation change in British chalk grasslands, Journal of Ecology, 94(2), 355-368, doi:10.1111/j.1365-2745.2006.01104.x.

Bense, V. F. F., T. Gleeson, S. E. E. Loveless, O. Bour, and J. Scibek (2013) Fault zone hydrogeology, Earth-Science Rev., 127, 171–192, doi:10.1016/j.earscirev.2013.09.008.

Bergstrom, A., K. Jencso, and B. McGlynn (2016), Spatiotemporal processes that contribute to hydrologic exchange between hillslopes, valley bottoms, and streams, Water Resour. Res., 52(6), 4628-4645.

Beven, K. J., and M. J. Kirkby (1979), A physically based, variable contributing area model of basin hydrology, Hydrological Sciences Bulletin, 24(1), 43-69, doi:10.1080/02626667909491834.

Beven, K. (1981), Kinematic subsurface stormflow, Water Resources Research, 17(5), 1419-1424.

Beven, K. (1997), Topmodel: A critique, Hydrological Processes, 11(9), 1069-1085.

Beven, K.J., and J. Freer (2001), A dynamic Topmodel, Hydrological Processes, 5(10), 1993-2011, doi.org/10.1002/hyp.252.

Beven, K. J. and Cloke, H. L. (2012), Comment on: Hyperresolution global land surface modeling: Meeting a grand challenge for monitoring Earth's terrestrial water by Eric F Wood et al. Water Resources Research, 48 (1). W01801. ISSN 0043-1397 doi: https://doi.org/10.1029/2011WR010982

1181 Blöschl, G. (2006), Hydrologic synthesis: Across processes, places, and scales, Water Resources Research, 42(3),
1182 W03S02, doi:10.1029/2005WR004319.

1183 Bonnet, M. P., et al. (2008), Floodplain hydrology in an Amazon floodplain lake (Lago Grande de Curuaí), Journal of
1184 Hydrology, 349(1), 18-30, doi:10.1016/j. jhydrol.2007.10.055.

1185 Borma, L. S., et al. (2009), Atmosphere and hydrological controls of the evapotranspiration over a floodplain forest
1186 in the Bananal Island region, Amazonia, J. Geophys. Res., 114, G01003, doi:10.1029/2007JG000641.

1187 Brantley S. L., T. S. White, A. F. White, D. Sparks, D Richter, K. Pregitzer, L. Derry L, J. Chorover, O. Chadwick, R.
1188 April, S. Anderson, R. Amundson R (2006), Frontiers in Exploration of the Critical Zone, Report of a workshop
1189 sponsored by National Science Foundation (NSF), October 24-26, 2005, Newark, DE, 30p.

1190 Brantley, S. L., et al. (2017c), Reviews and syntheses: on the roles trees play in building and plumbing the critical
1191 zone, Biogeosciences, 14, 5115-5142, https://doi.org/10.5194/bg-14-5115-2017.

1192 Brantley, S. L., M. I. Lebedeva, V. N. Balashov, K. Singha, P. L. Sullivan, and G. Stinchcomb (2017b), Toward a
1193 conceptual model relating chemical reaction fronts to water flow paths in hills, Geomorphology, 277, 100-117, doi:
1194 10.1016/j.geomorph.2016.09.027.

1195 Brantley, S. L., et al. (2017a), Designing a network of critical zone observatories to explore the living skin of the
1196 terrestrial Earth, Earth Surf. Dynam., 5(4), 841-860, doi:810.5194/esurf-5195-5841-2017.

1197 Brooks, P. D., J. Chorover, Y. Fan, S. E. Godsey, R. M. Maxwell, J. P. McNamara, and C. Tague (2015), Hydrological
1198 partitioning in the critical zone: Recent advances and opportunities for developing transferable understanding of
1199 water cycle dynamics, Water Resources Research, 51(9), 6973-6987.

1200 Brunke, M.A., P. Broxton, J. Pelletier, D. Gochis, P. Hazenberg, D.M. Lawrence, L.R. Leung, G. Niu, P.A. Troch, and X.
1201 Zeng (2016), Implementing and Evaluating Variable Soil Thickness in the Community Land Model, Version 4.5
1202 (CLM4.5). J. Climate, 29, 3441–3461, https://doi.org/10.1175/JCLI-D-15-0307.1.

1203 Bucci, S. J., F. G. Scholz, G. Goldstein, F. C. Meinzer, and M. E. J. O. Arce (2009), Soil water availability and rooting
1204 depth as determinants of hydraulic architecture of Patagonian woody species, Oecologia, 160(4), 631-641.

1205 Bucci, S. J., F. G .Scholz, G. Goldstein, W. A. Hoffmann, F. C. Meinzer, A. C. Franco, T. Giambelluca, and F. Miralles-
1206 Wilhelm (2008), Controls on stand transpiration and soil water utilization along a tree density gradient in a
1207 Neotropical savanna, Agricultural and Forest Meteorology, 148(6), 839-849.

1208 Buss, H. L., S. L. Brantley, F. N. Scatena, E. A. Bazilievskaya, A. Blum, M. Schulz, R. Jiménez, A. F. White, G. Rother,
1209 and D. Cole (2013), Probing the deep critical zone beneath the Luquillo Experimental Forest, Puerto Rico, Earth
1210 Surface Processes and Landforms, 38(10), 1170-1186.

1211 Cannon, W. A. (1911), The root habits of desert plants, Carnegie Institution of Washington.

1212 Cardenas, M. B., and X. W. Jiang (2010), Groundwater flow, transport, and residence times through topography-
1213 driven basins with exponentially decreasing permeability and porosity, Water Resour. Res., 46(11), W11538,
1214 doi:10.1029/2010WR009370.

1215 Chaney, N. W., M. H. Van Huijgevoort, E. Shevliakova, S. Malyshev, P. C. Milly, P. P. Gauthier, B. N. Sulman (2018),
1216 Harnessing big data to rethink land heterogeneity in Earth system models, Hydrol. Earth Syst. Sci., 22, 3311-3330,
1217 https://doi.org/10.5194/hess-22-3311-2018.

1218 Chen, Z., A. S. Auler, M. Bakalowicz, D. Drew, F. Griger, J. Hartmann, G. Jiang, N. Moosdorf, A. Richts, Z. Stevanovic,
1219 G., Veni, and N. Goldscheider (2017), The World Karst Aquifer Mapping project: concept, mapping procedure and
1220 map of Europe, Hydrogeol. J., 25(3), 771-785, doi:10.1007/s10040-016-1519-3.

1221 Clapp, R. B., and G. M. Hornberger (1978), Empirical equations for some soil hydraulic properties, Water Resour.
1222 Res., 14(4), 601-604, doi:10.1029/WR014i004p00601.

1223 Clark, D. B., and N. Gedney (2008), Representing the effects of subgrid variability of soil moisture on runoff
1224 generation in a land surface model, J. Geophys. Res., 113, D10111, doi:10.1029/2007JD008940.

1225 Clark, M. P., Y. Fan, D. M. Lawrence, J. C. Adam, D. Bolster, D. J. Gochis, R. P. Hooper, M. Kumar, L. R .Leung, and D.
1226 S. Mackay (2015), Improving the representation of hydrologic processes in Earth System Models, Water Resour.
1227 Res., 51(8), 5929-5956, doi:10.1002/2015WR017096.

1228 Clark, M. P., J. Hendrikx, A. G. Slater, D. Kavetski, B. Anderson, N. J. Cullen, T. Kerr, E. Ö. Hreinsson, and R. A. Woods
1229 (2011), Representing spatial variability of snow water equivalent in hydrologic and land-surface models: A review,
1230 Water Resour. Res., 47(7), https://doi.org/10.1029/2011WR010745.

1231 Cole, M. M. (1992), Influence of physical factors on the nature and dynamics of forest-savanna boundaries, in
1232 Nature and Dynamics of Forest-Savanna Boundaries (ed Furley PA, J Proctor, and J A Ratter), Chapman & Hall,
1233 Suffolk, UK 616 pages.

1234 Coomes, D. A., and P. J. Grubb (1996), Amazonian caatinga and related communities at La Esmeralda, Venezuela:
1235 forest structure, physiognomy and floristics, and control by soil factors, Vegetatio, 122(2), 167-191.

1236 Cullmann, J., W. J. Junk, G. Weber, and G. H. Schmitz (2006), The impact of seepage influx on cation content of a
1237 Central Amazonian floodplain lake, J. Hydrol., 328(1-2), 297-305, doi:10.1016/j.jhydrol.2005.12.027.

1238 Dawson, T. E., and J. S. Pate (1996), Seasonal water uptake and movement in root systems of Australian
1239 phraeatophytic plants of dimorphic root morphology: a stable isotope investigation, Oecologia, 107(1), 13-20.

1240 Day, F. P., and C. D. Monk (1974), Vegetation patterns on a southern Appalachian watershed, 55(5), Ecology.,
1241 1064-1074.

1242 Dearborn, K. D., and R. K. Danby (2017), Aspect and slope influence plant community composition more than
1243 elevation across forest–tundra ecotones in subarctic Canada, J Veg Sci, 28(3), 595-604, doi:10.1111/jvs.12521.

1244 Decharme, B., H. Douville, A. Boone, F. Habets, and J. Noilhan (2006), Impact of an exponential profile of saturated
1245 hydraulic conductivity within the ISBA LSM: simulations over the Rhône basin, J. Hydrometeorol., 7(1), 61-80.

1246 Decharme, B., R. Alkama, H. Douville, M. Becker, and A. Cazenave (2010), Global evaluation of the ISBA-TRIP
1247 continental hydrological system. Part II: Uncertainties in river routing simulation related to flow velocity and
1248 groundwater storage, J. Hydrometeorol., 11, 601–617, doi:10.1175/2010JHM1212.1.

1249 Dubs, B. (1992), Observations on the differentiation of woodland and wet savanna habitats in the Pantanal of
1250 Mato Grosso, Brazil, in Nature and Dynamics ff Forest-Savanna Boundaries (ed Furley PA, J Proctor, and J A Ratter),
1251 Chapman & Hall, Suffolk, UK 616 pages.

1252 Duffy, C. J. (1996), A two-state integral-balance model for soil moisture and groundwater dynamics in complex
1253 terrain, Water Resour. Res., 32(8), 2421-2434, doi: 10.1029/96WR01049.

1254 Dunne, T., and R. D. Black (1970), Partial area contributions to storm runoff in a small New England watershed,
1255 Water Resources Research, 6(5), 1296-1311.

1256 Ebel, B. A., K. Loague, J. E. Vanderkwaak, W. E. Dietrich, D. R. Montgomery, R. Torres, and S. P. Anderson (2007),
1257 Near-surface hydrologic response for a steep, unchanneled catchment near Coos Bay, Oregon: 2. Physics-based
1258 simulations, American Journal of Science, 307(4), 709-748, doi:10.2475/04.2007.03.

1259 Elliott, G. P., K. F. Kipfmueller (2010), Multi-scale influences of slope aspect and spatial pattern on ecotonal
1260 dynamics at upper treeline in the southern Rocky Mountains, USA, Antarctic, and Alpine Research, 42(1), 45-56.

1261 Elliott, G. P., C. M. Cowell (2015), Slope aspect mediates fine-scale tree establishment patterns at upper treeline
1262 during wet and dry periods of the 20th century, Antarctic, and Alpine Research, 47(4), 681-692.

1263 Eltahir, E. A., and P. J. F. Yeh (1999), On the asymmetric response of aquifer water level to floods and droughts in
1264 Illinois, Water Resour. Res., 35(4), 1199-1217.

1265 Endalamaw, A., W. Bolton, J. Young, D. Morton, L. Hinzman, and B. Nijssen (2017), Toward Improved
1266 Parameterization of a Meso-Scale Hydrologic Model in a Discontinuous Permafrost, Boreal Forest Ecosystem,
1267 Hydrol. Earth Syst. Sci., 21, 4663-4680, https://doi.org/10.5194/hess-21-4663-2017.

1268 Famiglietti, J., and E. Wood (1994), Multiscale modeling of spatially variable water and energy balance processes,
1269 Water Resources Research, 30(11), 3061-3078.

1270 Fan, Y., G. Miguez-Macho, E. G. Jobbágy, R. B. Jackson, and C. Otero-Casal (2017), Hydrologic regulation of plant
1271 rooting depth, Proceedings of the National Academy of Sciences of the United States of America, Vol 114, No 40,
1272 10572–10577, doi: 10.1073/pnas.1712381114.

1273 Fan, Y. (2015), Groundwater in the Earth's critical zone: Relevance to large-scale patterns and processes, Water
1274 Resources Research, 50yr Anniversary Special Issue, 51(5), 3052-3069, doi:10.1002/2015WR017037.

1275 Fan, Y., H. Li, and G. Miguez-Macho (2013), Global patterns of groundwater table depth, Science, 339(6122), 940-
1276 943, doi:10.1126/science.1229881.

1277 Fan, Y., and G. Miguez-Macho (2011), A simple hydrologic framework for simulating wetlands in climate and earth
1278 system models, Climate Dynamics, 37(1-2), 253-278, doi: 10.1007/s00382-010-0829-8.

1279 Fan, Y., G. Miguez-Macho, C. P. Weaver, R. Walko, and A. Robock (2007a), Incorporating water table dynamics in
1280 climate modeling, Part I: Water table observations and the equilibrium water table simulations, Journal of
1281 Geophysical Research-Atm, 112, D10125, doi:10.1029/2006JD008111.

1282 Fan, Y., L. Toran, and R. W. Schlische (2007b), Groundwater flow and groundwater-stream interaction in fractured
1283 and dipping sedimentary rocks: Insights from numerical models, Water Resources Research, 43, W01409,
1284 doi:10.1029/2006WR004864.

1285 Fan, Y., and R. L. Bras (1998), Analytical solutions to hillslope subsurface storm flow and saturation overland flow,
1286 Water Resources Research, 34(4), 921-927.

1287 FAO/IIASA/ISRIC/ISSCAS/JRC (2012), Harmonized World Soil Database (version 1.2). FAO, Rome, Italy and IIASA,
1288 Laxenburg, Austria.

1289 Faure, H., R. C. Walter, D. R. Grant, and P. Change (2002), The coastal oasis: ice age springs on emerged continental
1290 shelves, Glob. Planet. Change, 33(1-2), 47-56.

1291 Fisher, R. A., C. D. Koven, W. R. Anderegg, B. O. Christoffersen, M. C. Dietze, C. E. Farrior, J. A. Holm, G. C. Hurtt, R.
1292 G. Knox, and P. J. Lawrence (2018), Vegetation demographics in Earth System Models: A review of progress and
1293 priorities, Glob. Change Biol. 24(1), 35-54, https://doi.org/10.1111/gcb.13910.

1294 Flügel, W. A. (1995), Delineating hydrological response units by geographical information system analyses for
1295 regional hydrological modelling using PRMS/MMS in the drainage basin of the River Bröl, Germany, Hydrol.
1296 Processes, 9(3-4), 423-436, doi:10.1002/hyp.3360090313.

1297 Ford, D., and P. W. Williams (2007), Karst hydrogeology and geomorphology, ISBN:9780470849965 |Online
1298 ISBN:9781118684986 |DOI:10.1002/9781118684986, John Wiley & Sons Ltd, Chichester.

1299 Furley, P. A. (1992), Edaphic changes at the forest-savanna boundary with particular reference to the neotropics, in
1300 Nature and Dynamics of Forest-Savanna Boundaries (ed Furley PA, J Proctor, and J A Ratter), Chapman & Hall,
1301 Suffolk, UK 616 pages.

1302 Gaillardet, J., Braud, I., Hankard, F., Anquetin, S., Bour, O., Dorfliger, N., ... & Gourcy, L. (2018), OZCAR: the French
1303 network of critical zone observatories. Vadose Zone J, 17, 180067, 10.2136/vzj2018.04.0067.

1304 Genereux, D. P., and M. Jordan (2006), Interbasin groundwater flow and groundwater interaction with surface
1305 water in a lowland rainforest, Costa Rica: a review, J. Hydrol., 320(3-4), 385-399,
1306 doi:10.1016/j.jhydrol.2005.07.023.

1307 Genereux, D. P., M. T. Jordan, and D. Carbonell (2005), A paired-watershed budget study to quantify interbasin
1308 groundwater flow in a lowland rain forest, Costa Rica, Water Resour. Res., 41(4), W04011,
1309 doi:10.1029/2004WR003635.

1310 Genereux, D. P., S. J. Wood, and C. M. Pringle (2002), Chemical tracing of interbasin groundwater transfer in the
1311 lowland rainforest of Costa Rica, J. Hydrol., 258(1-4), 163-178, doi:10.1016/S0022-1694(01)00568-6.

1312 van Genuchten M. T. (1980), A closed-form equation for predicting the hydraulic conductivity of unsaturated soils.
1313 Soil Science Society of America Journal. 44 (5): 892–898.

1314 Geroy, I., M. Gribb, H.-P. Marshall, D. Chandler, S. G. Benner, and J. McNamara (2011), Aspect influences on soil
1315 water retention and storage, Hydrol. Process., 25(25), 3836-3842, doi:10.1002/hyp.8281.

1316 Gilbert, G. K. (1909), The convexity of hilltops, Journal of Geology, 17(4), 344-350.

1317 Gleeson, T., N. Moosdorf, J. Hartmann, and L. Van Beek (2014), A glimpse beneath earth's surface: GLobal
1318 HYdrogeology MaPS (GLHYMPS) of permeability and porosity, Geophyscial Research Letters, 41(11), 3891-3898,
1319 doi: 10.1002/2014gl059856.

1320 Gleeson, T., K. M. Befus, S. Jasechko, E. Luijendijk, and M. B. Cardenas (2016), The global volume and distribution
1321 of modern groundwater, Nature Geosci., 9(2), 161.

1322 Godsey, S. E., and J. W. Kirchner (2014), Dynamic, discontinuous stream networks: hydrologically driven variations
1323 in active drainage density, flowing channels and stream order, Hydrol. Process., 28(23), 5791-5803, doi:
1324 10.1002/hyp.10310.

1325 Godsey, S. E., J. W. Kirchner, and D. W. Clow (2009), Concentration–discharge relationships reflect chemostatic
1326 characteristics of US catchments, Hydrol. Process., 23(13), 1844-1864, doi:10.1002/hyp.7315.

1327 Goodfellow, B. W., O. A. Chadwick, G. E. Hilley, and Landforms (2014), Depth and character of rock weathering
1328 across a basaltic-hosted climosequence on Hawai ‘i, Earth Surf. Process. Landforms, 39(3), 381-398,
1329 doi:10.1002/esp.3505.

1330 Goteti, G., J. S. Famiglietti, and K. Asante (2008), A Catchment-Based Hydrologic and Routing Modeling System with
1331 explicit river channels, J. Geophys. Res., 113, D14116, doi:10.1029/2007JD009691. .

1332 Goulden, M., R. Anderson, R. Bales, A. Kelly, M. Meadows, and G. Winston (2012), Evapotranspiration along an
1333 elevation gradient in California's Sierra Nevada, Journal of Geophysical Research, 117, G03028–G03709.

1334 Graham R. C., A. Rossi, K. R. Hubbert (2010), Rock to regolith conversion: producing hospitable substrates for
1335 terrestrial ecosystems, GSA Today, 20, 4–9.

1336 Grogan, J., and J. Galvão (2006), Physiographic and floristic gradients across topography in transitional seasonally
1337 dry evergreen forests of southeast Pará, Brazil, Acta Amazon, 36(4), 483-496.

1338 Groves, C., and J. Meiman (2005), Weathering, geomorphic work, and karst landscape evolution in the Cave City
1339 groundwater basin, Mammoth Cave, Kentucky, Geomorphology, 67(1-2 SPEC. ISS.), 115-126,
1340 doi:10.1016/j.geomorph.2004.07.008.

1341 Hales, T., C. Ford, T. Hwang, J. M. Vose, and L. E. Band (2009), Topographic and ecologic controls on root
1342 reinforcement, J. Geophys. Res., 114, F03013, doi:10.1029/2008JF001168.

1343 Harbaugh, A. W., E. R. Banta, M. C. Hill, and M. G. McDonald (2000), Modflow-2000, the U.S. Geological Survey
1344 modular groundwater model—User guide to modularization concepts and the groundwater flow process, U.S.
1345 Geol. Surv., Open File Rep., 00-92.

1346 Harper, A. B., A. S. Denning, I. T. Baker, M. D. Branson, L. Prihodko, and D. A. Randall (2010), Role of deep soil
1347 moisture in modulating climate in the Amazon rainforest, Geophys. Res. Lett., 37, L05802,
1348 doi:10.1029/2009GL042302.

1349 Hartmann, A., T. Gleeson, Y. Wada, and T. Wagener (2017), Enhanced groundwater recharge rates and altered
1350 recharge sensitivity to climate variability through subsurface heterogeneity, Proc. Natl. Acad. Sci., 114(11), 2842-
1351 2847, doi: 10.1073/pnas.1614941114.

1352 Hartmann, A. (2016), Putting the cat in the box: why our models should consider subsurface heterogeneity at all
1353 scales, WIREs Water, 3(4), 478-486, doi:10.1002/wat2.1146.

1354 Hartmann, A., T. Gleeson, R. Rosolem, F. Pianosi, Y. Wada, and T. Wagener (2015), A large-scale simulation model
1355 to assess karstic groundwater recharge over Europe and the Mediterranean, Geosci. Model Dev., 8(6), 1729–1746,
1356 doi:10.5194/gmd-8-1729-2015.

1357 Hartmann, J., and N. Moosdorf (2012), The new global lithological map database GLiM: A representation of rock
1358 properties at the Earth surface, Geophys. Geosyst., 13, Q12004, doi: 10.1029/2012GC004370.

1359 Hazenberg, P., Y. Fang, P. Broxton, D. Gochis, G. Y. Niu, J. Pelletier, P. A. Troch ,and X. Zeng (2015), A hybrid-3D
1360 hillslope hydrological model for use in Earth system models, Water Resour. Res., 51(10), 8218–8239,
1361 doi:10.1002/2014WR016842.

1362 Heidbach, O., M. Rajabi, K. Reiter, M. Ziegler, WSM Team (2016) World Stress Map Database Release 2016, GFZ
1363 Data Services, doi:10.5880/WSM.2016.001.

1364 Heimsath, A. M., W. E. Dietrich, K. Nishiizumi, and R. Finkel (1997), The soil production function and landscape
1365 equilibrium, Nature, 388 (6640), 358–361.

1366 Hengl, T., J. de Jesus, G. Heuvelink, M. Gonzalez, M. Kilibarda, A. Blagotic and et al. (2017), Soilgrids250m: Global
1367 gridded soil information based on machine learning, PloS one, 12 (2), e0169748,
1368 doi:10.1371/journal.pone.0169748.

1369 Hewlett, J. D., and A. R. Hibbert (1967), Factors affecting the response of small watersheds to precipitation in
1370 humid areas, Proc. First International Forest Hydrology Symposium, 275-290.

1371 Hodnett, M., I. Vendrame, O. Marques Filho, A. De, M. Oyama, and J. Tomasella (1997a), Soil water storage and
1372 groundwater behaviour in a catenary sequence beneath forest in central Amazonia: I. Comparisons between
1373 plateau, slope and valley floor, Hydrol. Earth Syst. Sci., 1, 265–277, doi:10.5194/hess-1-265-1997.

1374 Hodnett, M., I. Vendrame, O. Marques Filho, A. De, M. Oyama, J. Tomasella (1997b), Soil water storage and
1375 groundwater behaviour in a catenary sequence beneath forest in central Amazonia. II. Floodplain water table
1376 behaviour and implications for streamflow generation, Hydrol. Earth Syst. Sci., 1, 279–290, doi:10.5194/hess-1-
1377 279-1997.

1378 Holbrook, W. S., C. S. Riebe, M. Elwaseif, J. L. Hayes, K. Basler-Reeder, D. L. Harry, A. Malazian, A. Dosseto, P. C.
1379 Hartsough, and J. W. Hopmans (2014), Geophysical constraints on deep weathering and water storage potential in
1380 the Southern Sierra Critical Zone Observatory, Earth Surf. Process. Landforms, 39: 366–380. doi:10.1002/esp.3502.

1381 Hooke, R. L. (2000), Toward a uniform theory of clastic sediment yield in fluvial systems, Geol. Soc. Am. Bull., 112,
1382 1778– 1786.

1383 Hopp, L., and J. J. McDonnell (2009), Connectivity at the hillslope scale: Identifying interactions between storm
1384 size, bedrock permeability, slope angle and soil depth, Journal of Hydrology, 376, 378-391, DOI:
1385 10.1016/j.jhydrol.2009.07.047.

1386 Howard, A. (1925), The effect of grass on trees, Proc. Royal. Soc. B, 97,284–321.

1387 Hoylman, Z. H., K. G. Jencso, J. Hu, J. T. Martin, Z. A. Holden, C. A. Seielstad, and E. M. Rowell (2018), Hillslope
1388 Topography Mediates Spatial Patterns of Ecosystem Sensitivity to Climate, Journal of Geophysical Research:
1389 Biogeosciences, 123, 353–371. https://doi.org/10.1002/2017JG004108.

1390 von Humboldt, A. (1807), Essay on the Geography of Plants (English Translation 2009), The University of Chicago
1391 Press. 296 pages.

1392 Huscroft, J., T. Gleeson, J. Hartmann, and J. Börker (2018), Compiling and mapping global permeability of the
1393 unconsolidated and consolidated Earth: GLobal HYdrogeology MaPS 2.0 (GLHYMPS 2.0), Geophysical Research
1394 Letters, 45(4), 1897–1904. https://doi.org/10.1002/2017GL075860.

1395 Hwang, T., L. Band, and T. Hales (2009), Ecosystem processes at the watershed scale: Extending optimality theory
1396 from plot to catchment, Water Resour. Res., 45, W11425, doi:10.1029/2009WR007775.

1397 Jasechko, S., Kirchner, J. W., Welker, J. M., and McDonnell, J. J. (2016), Substantial proportion of global streamflow
1398 less than three months old, Nat. Geosci., 9(2): 126-129.

1399 Jencso, K. G., B. L. McGlynn, M. N. Gooseff, S. M. Wondzell, K. E. Bencala, and L. A. Marshall (2009), Hydrologic
1400 connectivity between landscapes and streams: Transferring reach-and plot-scale understanding to the catchment
1401 scale, Water Resour. Res., 45, W04428, doi:10.1029/2008WR007225.

1402 Jiang, X. W., L. Wan, X. S. Wang, S. Ge, and J. Liu (2009), Effect of exponential decay in hydraulic conductivity with
1403 depth on regional groundwater flow, Geophys. Res. Lett., 36, L24402, doi:10.1029/2009GL041251.

1404 Jiang, X.-W., X.-S. Wang, and L. Wan (2010), Semi-empirical equations for the systematic decrease in permeability
1405 with depth in porous and fractured media, Hydrogeol. J., 18(4), 839–850

1406 Jirka, S., A. J. McDonald, M. S. Johnson, T. R. Feldpausch, E. G. Couto, and S. J. Riha (2007), Relationships between
1407 soil hydrology and forest structure and composition in the southern Brazilian Amazon, J. Veg. Sci., 18, 183–197.

1408 Jobbagy, E. G., M. D. Nosetto, P. E. Villagra, and R. B. Jackson (2011), Water subsidies from mountains to deserts:
1409 Their role in sustaining groundwater-fed oases in a sandy landscape, Ecol. Appl., 21, 678–694.

1410 Johnson A. K. (1848), The Physical Atlas of Natural Phenomena: Reduced from the Edition in Imperial Folio for the
1411 Use of Colleges, Academies and Families, author Alexander Keith Johnston, publisher W. Blackwood, 1850.

1412 Johnson, D. M., J. C. Domec, Z. C. Berry, A. M. Schwantes, D. R. Woodruff, K. A. McCulloh, H. W. Polley, R.
1413 Wortemann, J. J. Swenson, D. S. Mackay, N. G. McDowell, and R. B. Jackson (2018), Co-occurring woody species
1414 have diverse hydraulic strategies and mortality rates during an extreme drought. Plant, Cell and Environment,
1415 41(3), 576-588, doi:10.1111/pce.13121.

1416 Kim, Y., and E. A. B. Eltahir (2004), Role of topography in facilitating coexistence of trees and grasses within
1417 savannas, Water Resour. Res., 40, W07505, doi:10.1029/2003WR002578.

1418 Kimber P. C. (1974), The Root System of Jarrah (Eucalyptus marginata) (Forests Department of Western Australia,
1419 Perth, WA, Australia), Research Papers No. 10.

1420 Kirchner, J.W., X.H. Feng, and C. Neal (2001), Catchment-scale advection and dispersion as a mechanism for fractal
1421 scaling in stream tracer concentrations, Journal of Hydrology, 254, 81-100.

1422 Kirchner, J. W., Colin Neal (2013), Universal fractal scaling in water quality. Proceedings of the National Academy of
1423 Sciences, 110 (30:) 12213-12218; DOI: 10.1073/pnas.1304328110

1424 Kleidon, A., M. Heimann (1998), A method of determining rooting depth from a terrestrial biosphere model and its
1425 impacts on the global water and carbon cycle, Glob. Change Biol., 4, 275–286, http://dx.doi.org/10.1046/j.1365-
1426 2486.1998. 00152.x

1427 Kleidon, A., and M. Heimann (2000), Assessing the role of deep rooted vegetation in the climate system with
1428 model simulations: Mechanism, comparison to observations and implications for Amazonian deforestation, Clim.
1429 Dyn., 16, 183–199, doi:10.1007/s003820050012.

1430 Klos, P. Z., M. L. Goulden, C. S. Riebe, C. L. Tague, A. T. O'Geen, B. A. Flinchum, et al. (2018), Subsurface plant-
1431 accessible water in mountain ecosystems with a Mediterranean climate, Wiley Interdisciplinary Reviews: Water,
1432 5(3), e1277.

1433 Koster, R., and M. Suarez (1992), Modeling the land surface boundary in climate models as a composite of
1434 independent vegetation stands, J. Geophys. Res., 97, 2697–2715, doi:10.1029/91JD01696.

1435 Koster, R. D., M. J. Suarez, A. Ducharne, M. Stieglitz, and P. Kumar (2000), A catchment-based approach to
1436 modeling land surface processes in a general circulation model: 1. Model structure, J. Geophys. Res., 105, 24,809–
1437 24,822, doi:10.1029/2000JD900327.

1438 Krakauer, N. Y., H. Li, and Y. Fan (2014), Groundwater flow across spatial scales: Importance for climate modeling,
1439 Environmental Research Letters, 9, 034003.

1440 Krause, H., S. Rieger, and S. A. Wilde (1959), Soils and forest growth on different aspects in the Tanana watershed
1441 of interior Alaska, Ecology, 40: 492-495. doi:10.2307/1929774

1442 Kuang, X., and J. J. Jiao (2014), An integrated permeability-depth model for Earth's crust, Geophys. Res. Lett., 41,
1443 7539–7545, doi:10.1002/2014GL061999.

1444 Kuppel, S., Y. Fan, and E. G. Jobbagy (2017), Seasonal hydrologic buffer on continents: patterns, drivers and
1445 ecological benefits, Advances in Water Resources, 102: 178-187, doi:10.1016/j.advwatres.2017.01.004.

1446 Lanni, C., J. McDonnell, and R. Rigon (2011), On the relative role of upslope and downslope topography for
1447 describing water flow path and storage dynamics: a theoretical analysis, Hydrological Processes, 25(25), 3909-
1448 3923, DOI: 10.1002/hyp.8263.

1449 Lebedeva, M. I., and S. L. Brantley (2017), Weathering and erosion of fractured bedrock systems, Earth Surf.
1450 Process. Landforms, 42: 2090–2108. doi: 10.1002/esp.4177.

1451 Lee, J. E., R. S. Oliveira, T. E. Dawson, and I. Fung (2005), Root functioning modifies seasonal climate, Proc. Natl.
1452 Acad. Sci.U. S. A., 102(49), 17576-17581.

Lehner, B., and G. Grill (2013): Global river hydrography and network routing: baseline data and new approaches to study the world's large river systems. Hydrological Processes, 27(15): 2171–2186. Data is available at www.hydrosheds.org.

Leng G., M. Huang, Q. Tang, W.J. Sacks, H. Lei, and L.R. Leung (2013), Modeling the Effects of Irrigation on Land Surface Fluxes and States over the Conterminous United States: Sensitivity to Input Data and Model Parameters. Journal of Geophysical Research. D. (Atmospheres) 118 (17): 9789-9803. doi:10.1002/jgrd.50792

Lesack, L. F., and J. M. Melack (1995), Flooding hydrology and mixture dynamics of lake water derived from multiple sources in an Amazon floodplain lake, Water Resour. Res., 31, 329–345, doi:10.1029/94WR02271.

Lesack, L. F. (1995), Seepage exchange in an Amazon floodplain lake, Limnol. Oceanogr., 40, 598–609, doi:10.4319/lo.1995.40.3.0598.

Liston, G.E. (2004), Representing Subgrid Snow Cover Heterogeneities in Regional and Global Models. J. Climate, 17: 1381–1397, https://doi.org/10.1175/1520-0442(2004)017<1381:RSSCHI>2.0.CO;2.

Liu, Y. Y., D. R .Maidment, D. G. Tarboton, X. Zheng, and S. Wang (2018), A CyberGIS Integration and Computation Framework for High-Resolution Continental-Scale Flood Inundation Mapping, JAWRA Journal of the American Water Resources Association, 54(4): 770-784, https://doi.org/10.1111/1752-1688.12660.

Longenecker, J., T. Bechtel, Z. Chen, N. Goldscheider, T. Liesch, and R. Walter (2017), Correlating Global Precipitation Measurement satellite data with karst spring hydrographs for rapid catchment delineation, Geophys. Res. Lett., 44(10), 4926–4932, doi:10.1002/2017GL073790.

Lovill, S. M., W. J. Hahm, and W. E. Dietrich (2018), Drainage from the critical zone: Lithologic controls on the persistence and spatial extent of wetted channels during the summer dry season, Water Resources Research, 54, https://doi.org/10.1029/2017WR021903.

Mankin, J. S., J. E. Smerdon, B. I. Cook, A. P. Williams, and R. Seager (2017), The curious case of projected twenty-first-century drying but greening in the American West, J. Climate, 30, 8689–8710, https://doi.org/10.1175/JCLI-D-17-0213.1.

Manning, C. E., and S. E. Ingebritsen (1999), Permeability of the continental crust: Implications of geothermal data and metamorphic systems, Rev. Geophys., 37(1), 127–150, doi: 10.1029/1998RG900002.

Marani, M., E. Eltahir, and A. Rinaldo (2001), Geomorphic controls on regional base flow, Water Resour. Res., 37, 2619–2630, doi:10.1029/2000WR000119.

Markewitz, D., S. Devine, E. A. Davidson, P. Brando, and D. C. Nepstad (2010), Soil moisture depletion under simulated drought in the Amazon: impacts on deep root uptake, New Phytol., 187, 592–607, doi:10.1111/j.1469-8137.2010.03391.x.

Martinez, J. A., F. Dominguez, and G. Miguez-Macho (2016), Effects of a groundwater scheme on the simulation of soil moisture and evapotranspiration over southern South America, J. Hydrometeor., 17, 2941–2957, https://doi.org/10.1175/JHM-D-16-0051.1.

Maxwell, R. M., F. K. Chow, and S. J. Kollet (2007), The groundwater-land-surface-atmosphere connection: Soil moisture effects on the atmospheric boundary layer in fully-coupled simulations, Adv. Water Resour., 30(12), 2447–2466, doi:10.1016/j.advwatres.2007.05.018.

Maxwell, R. M., and S. J. Kollet (2008), Interdependence of groundwater dynamics and land-energy feedbacks under climate change, Nat. Geosci., 1(10), 665–669.

Maxwell, R. M., and L. E. Condon (2016), Connections between groundwater flow and transpiration partitioning, Science, 353(6297), 377-380, DOI: 10.1126/science.aaf7891.

McCarthy, T. S. (2006) ,Groundwater in the wetlands of the Okavango Delta, Botswana, and its contribution to the structure and function of the ecosystem, J. Hydrol., 320, 264–282, doi:10.1016/j.jhydrol.2005.07.045.

McDonnell, J. J. (1990), A rationale for old water discharge through macropores in a steep, humid catchment, Water Resources Research 26(11): 2821-2832.

McDonnell, J. J. (2014), The two water worlds hypothesis: ecohydrological separation of water between streams and trees?, WIREs Water, 1: 323-329. doi:10.1002/wat2.1027.

McDonnell, J. J., and R. Woods (2004), On the need for catchment classification, Journal of Hydrology, 299, 2-3.

McGuire, K. J., and J. J. McDonnell (2010), Hydrological connectivity of hillslopes and streams: Characteristic time scales and nonlinearities, Water Resour. Res., 46, W10543, doi: 10.1029/2010WR009341.

McLaughlin, B. C., D. D. Ackerly, P. Z. Klos, J. Natali ,T. E. Dawson, and S. E. Thompson (2017), Hydrologic refugia, plants, and climate change, Global Change Biology 23(8), 2941-2961.

Tromp-van Meerveld, H. J., and J. J. McDonnell (2006), Threshold relations in subsurface stormflow: 1. A 147-storm analysis of the Panola hillslope, Water Resour. Res., 42, W02410, doi: 10.1029/2004WR003778.

Meerveld, I. T., and M. Weiler (2008), Hillslope dynamics modeled with increasing complexity, J. Hydrol., 361(1–2), 24–40, doi:10.1016/j.jhydrol.2008.07.019.

Meinzer, O. E. (1927), Plants as indicators of ground water, U.S. Geol. Surv. Water Supply Pap. 577, 115 pp., U.S. Govern. Print. Off., Washington,D. C.

Mezentsev, V. J. (1955), More on the calculation of average total evaporation, Meteorol. Gidrol., 5, 24-26.

Miguez-Macho, G., and Y. Fan (2012a), The role of groundwater in the Amazon water cycle: 1. Influence on seasonal streamflow, flooding and wetlands, J. Geophys. Res. 117, D15113, doi:10.1029/2012JD017539.

Miguez-Macho, G., and Y. Fan (2012b), The role of groundwater in the Amazon water cycle: 2. Influence on seasonal soil moisture and evapotranspiration, J. Geophys. Res. 117, D15114, doi:10.1029/2012JD017540.

Miller, G. R., X. Chen, Y. Rubin, S. Ma, and D. D. Baldocchi (2010), Groundwater uptake by woody vegetation in a semiarid oak savanna, Water Resources Research 46(10): 273-214.

Milly, P. C. D., and K. A. Dunne (1994), Sensitivity of the global water cycle to the water-holding capacity of land, J. Climate, 7, 506–526, https://doi.org/10.1175/1520-0442(1994)007<0506:SOTGWC>2.0.CO;2.

Milly, P.C. and A.B. Shmakin (2002), Global modeling of land water and energy balances. part i: the land dynamics (lad) model. J. Hydrometeor., 3, 283–299, https://doi.org/10.1175/1525-541(2002)003<0283:GMOLWA>2.0.CO;2

Milly, P. C. D., S. L. Malyshev, E. Shevliakova, K. A. Dunne, K. L. Findell, T. Gleeson, Z. Liang, P. Phillipps, R. J. Stouffer, and S. Swenson (2014), An enhanced model of land water and energy for global hydrologic and earth-system studies, J. Hydrometeorol., 15(5), 1739-1761, https://doi.org/10.1175/JHM-D-13-0162.1.

Mohamed, Y., H. Savenije, W. Bastiaanssen, B. J. H. Van den Hurk (2006), New lessons on the Sudd hydrology learned from remote sensing and climate modeling, Hydrol. Earth Syst. Sci., 10, 507–518, doi:10.5194/hess-10-507-2006.

Montgomery ,D. R., and W. E. Dietrich (1988), Where do channels begin?, Nature, 336(6196), 232-234.

Montgomery, D. R., W. E. Dietrich, R. Torres, S. P. Anderson, and J. T. Heffner (1997), Hydrologic response of a steep, unchanneled valley to natural and applied rainfall, Water Resources Research, 33(1), 91-109.

Moulatlet, G. M., F. R. Costa, C. D. Rennó, T. Emilio, and J. Schietti (2014), Local hydrological conditions explain floristic composition in lowland Amazonian forests, Biotropica, 46: 395–403. doi: 10.1111/btp.12117.

Nepstad, D. C., C. R. de Carvalho, E. A. Davidson, P. H. Jipp, P. A. Lefebvre, G. H. Negreiros, E. D. da Silva, T. A. Stone, S. E. Trumbore, and S. Vieira (1994), The role of deep roots in the hydrological and carbon cycles of Amazonian forests and pastures, Nature, 372, 666–669, doi:10.1038/372666a0.

Neu ,V., C. Neill, and A. V. Krusche (2011), Gaseous and fluvial carbon export from an Amazon forest watershed, Biogeochemistry, 105, 133–147, doi:10.1007/s10533-011-9581-3.

Newman, A. J., M. P. Clark, A. Winstral, D. Marks, and M. Seyfried (2014), The use of similarity concepts to represent subgrid variability in land surface models: Case study in a snowmelt-dominated watershed, Journal of Hydrometeorology, 15(5), 1717-1738.

Nijssen, B., D. P. Lettenmaier, X. Liang, S. W. Wetzel, and E. F. Wood (1997), Streamflow simulation for continental-scale river basins, . Water Resour. Res., 33, 711–724, doi:10.1029/96WR03517.

Nippgen, F., B. L. McGlynn, and R. E. Emanuel (2015), The spatial and temporal evolution of contributing areas, Water Resources Research, 51(6), 4550-4573.

1545 Niu, G. Y., Z. L. Yang, R. E. Dickinson, and L. E. Gulden (2005), A simple TOPMODEL-based runoff parameterization
1546 (SIMTOP) for use in global climate models, , J. Geophys. Res., 110, D21106, doi: 10.1029/2005JD006111.

1547 Nobre, A. D., L. A. Cuartas, M. Hodnett, C .D. Rennó, G. Rodrigues, A. Silveira, M. Waterloo, and S. Saleska (2011),
1548 Height Above the Nearest Drainage–a hydrologically relevant new terrain model, J. Hydrol., 404(1-2), 13-29.

1549 Ogden, F. L., T. D. Crouch, R. F. Stallard, and J. S. Hall (2013), Effects of land cover and use on dry season river
1550 runoff, runoff efficiency, and peak storm runoff in the seasonal tropics of Central Panama, Water Resour. Res., 49,
1551 8443–8462, doi: 10.1002/2013WR013956.

1552 Ollier, C., and C. Pain (1996), Regolith, soils and landforms, ISBN: 978-0-471-96121-5, 326 pages, Wiley: Chichester.

1553 Paola, C., E. Foufoula-Georgiou, W. E. Dietrich, M. Hondzo, D. Mohrig, G. Parker, M. E. Power, I. Rodriguez-Iturbe,
1554 V. Voller, and P. Wilcock (2006), Toward a unified science of the Earth's surface: Opportunities for synthesis among
1555 hydrology, geomorphology, geochemistry, and ecology, Water Resour. Res., 42, W03S10, doi:
1556 10.1029/2005WR004336.

1557 Pavlis, J., and J. Jeník (2000), Roots of pioneer trees in the Amazonian rain forest, Trees (Berl), 14(8), 442-455.

1558 Pelletier, J. D., P. D. Broxton, P. Hazenberg, X. Zeng, P. A. Troch, G. Y. Niu, Z. Williams, M. A. Brunke, and D. Gochis
1559 (2016), A gridded global data set of soil, intact regolith, and sedimentary deposit thicknesses for regional and
1560 global land surface modeling, J. Adv. Model. Earth Syst., 8, 41–65, doi:10.1002/2015MS000526.

1561 Pelletier, J.D., G. A. Barron-Gafford, H. Gutiérrez-Jurado, E. L. S. Hinckley, E. Istanbulluoglu, L. A. McGuire, G. Y. Niu,
1562 M. J. Poulos, C. Rasmussen, P. Richardson and T. L. Swetnam (2018), Which way do you lean? Using slope aspect
1563 variations to understand Critical Zone processes and feedbacks, Earth Surface Processes and Landforms, 43(5),
1564 1133-1154.

1565 Perdrial, J., P. D. Brooks, T. Swetnam, K. A. Lohse, C. Rasmussen, M. Litvak, A. A. Harpold, X. Zapata-Rios, P.
1566 Broxton, and B. Mitra (2018), A net ecosystem carbon budget for snow dominated forested headwater
1567 catchments: linking water and carbon fluxes to critical zone carbon storage, Biogeochemistry, 138(3), 225-243,
1568 https://doi.org/10.1007/s10533-018-0440-3.

1569 Ping, C., G. Michaelson, E. Packee, C. Stiles, D. Swanson, and K. Yoshikawa (2005), Soil catena sequences and fire
1570 ecology in the boreal forest of Alaska, Contribution from Agricultural and Forestry Experiment Station, UAF
1571 SNRAS/AFES Pub. No. 2005-003, Soil Sci. Soc. Am. J., 69(6), 1761-1772, doi:10.2136/sssaj2004.0139.

1572 Pokhrel, Y. N., Y. Fan, G. Miguez-Macho, P. J. F. Yeh, and S. C. Han (2013), The role of groundwater in the Amazon
1573 water cycle: 3. Influence on terrestrial water storage computations and comparison with GRACE, J. Geophys. Res.
1574 Atmos., 118(8), 3233-3244, doi:10.1002/jgrd.50335.

1575 Rahman, M., R. Rosolem (2017), Towards a simple representation of chalk hydrology in land surface modelling,
1576 Hydrology and Earth System Sciences, 21, 459-471.

Ratter J. A. (1992), Transitions between cerrado and forest vegetation in Brazil, in Nature and Dynamics of Forest-Savanna Boundaries (ed Furley PA, J Proctor, and J A Ratter), Chapman & Hall, Suffolk, UK 616 pages.

Rempe, D. M., and W. E. Dietrich (2014), A bottom-up control on fresh-bedrock topography under landscapes, Proceedings of the National Academy of Sciences, 201404763.

Rempe, D. M., and W. E. Dietrich (2018), Direct observations of rock moisture, a hidden component of the hydrologic cycle, Proceedings of the National Academy of Sciences ,115(11), 2664-2669, DOI: 10.1073/pnas.1800141115.

Richey, J. E., C. Nobre, and C. Deser (1989a), Amazon River discharge and climate variability: 1903 to 1985, Science, 246, 101–103, doi:10.1126/ science.246.4926.101.

Richey, J. E., L. A. Mertes, T. Dunne, R. L. Victoria, B. R. Forsberg, A. C. Tancredi, and E. Oliveira (1989b), Sources and routing of the Amazon River flood wave, Global Biogeochem. Cycles, 3, 191–204, doi:10.1029/GB003i003p00191.

Richey, J. E., M. V. Ballester, E. A. Davidson, M. S. Johnson, and A. Krusche (2011), Land-Water interactions in the Amazon, Biogeochemistry, 105, 1-5, doi:10.1007/s10533-011-9622-y.

Riebe, C. S., W. J. Hahm, S. L. Brantley, and Landforms (2017), Controls on deep critical zone architecture: A historical review and four testable hypotheses, Earth Surf. Process. Landforms, 42: 128–156. doi: 10.1002/esp.4052.

Roering, J. J., J. Marshall, A. M. Booth, M. Mort, and Q. Jin (2010), Evidence for biotic controls on topography and soil production, Earth and Planetary Science Letters 298(1-2), 183–190.

Rossatto, D. R., L. de Carvalho Ramos Silva, R. Villalobos-Vega, L. d. S. L. Sternberg, and A. C. Franco (2012), Depth of water uptake in woody plants relates to groundwater level and vegetation structure along a topographic gradient in a neotropical savanna, Environmental and Experimental Botany, 77, 259-266.

Rouholahnejad-Freund, E., and J. W. Kirchner (2017), A Budyko framework for estimating how spatial heterogeneity and lateral moisture redistribution affect average evapotranspiration rates as seen from the atmosphere, Hydrology and Earth System Sciences, 21(1), 217-233.

Saar, M. O., and M. Manga (2004), Depth dependence of permeability in the Oregon Cascades inferred from hydrogeologic, thermal, seismic, and magmatic modeling constraints, Journal of Geophysical Research: Solid Earth, 109, B04204, doi:10.1029/2003JB002855.

Sakata, Y., and R. Ikeda (2013), Depth dependence and exponential models of permeability in alluvial-fan gravel deposits, Hydrogeology Journal, 21(4), 773-786, https://doi.org/10.1007/s10040-013-0961-8.

Salve, R., D. M. Rempe, and W. E. Dietrich (2012), Rain, rock moisture dynamics, and the rapid response of perched groundwater in weathered, fractured argillite underlying a steep hillslope, Water Resources Research, 48(11), W11528, DOI: 10.1029/2012WR012583.

Schaller, M. F., and Y. Fan (2009), River basins as groundwater exporters and importers: Implications for water cycle and climate modeling, Journal of Geophysical Research: Atmospheres, 114, D04103, doi: 10.1029/2008 JD010636.

Schietti, J., et al. (2014), Vertical distance from drainage drives floristic composition changes in an Amazonian rainforest, Plant Ecology & Diversity, 7(1-2), 241-253, DOI: 10.1080/17550874.2013.783642.

Schimper, A. F. W.(1903), Plant-geography upon a physiological basis, Oxford:Clarendon Press. doi:10.5962/bhl.title.8099

Schwantes, A. M., A. J. Parolari, J. J. Swenson, D. M. Johnson, J.-C. Domec, R. B. Jackson, N. Pelak, and A. Porporato (2018), Accounting for landscape heterogeneity improves spatial predictions of tree vulnerability to drought, New Phytologist, 220(1), 132-146, https://doi.org/10.1111/nph.15274.

Sellers, P. J., D. A. Randall, G. J. Collatz, J. A. Berry, C. B. Field, D. A. Dazlich, C. Zhang, G. D. Collelo, and L. Bounoua (1996a), A Revised Land Surface Parameterization (SiB2) for Atmospheric GCMS. Part I: Model Formulation, Journal of Climate, 9(4), 676-705.

Sellers, P. J., C. J. Tucker, G. J. Collatz, S. O. Los, C. O. Justice, D. A. Dazlich, and D. A. Randall (1996b), A Revised Land Surface Parameterization (SiB2) for Atmospheric GCMS. Part II: The Generation of Global Fields of Terrestrial Biophysical Parameters from Satellite Data, Journal of Climate, 9(4), 706-737.

Shen, C., W. J. Riley, K. R. Smithgall, J. M. Melack, and K. Fang (2016), The fan of influence of streams and channel feedbacks to simulated land surface water and carbon dynamics, Water Resources Research, 52(2), 880-902, doi:10.1002/2015WR018086.

Shi, Y., D. M. Eissenstat, Y. He, and K. J. Davis (2018), Using a spatially-distributed hydrologic biogeochemistry model with a nitrogen transport module to study the spatial variation of carbon processes in a Critical Zone Observatory, Ecological Modelling, 380, 8-21, DOI: 10.1016/j.ecolmodel.2018.04.007.

Shmonov, V. M., V. M. Vitiovtova, A. V. Zharikov, and A. A. Grafchikov (2003), Permeability of the continental crust: implications of experimental data, Journal of Geochemical Exploration, 78-79, 697-699.

Slim, M., J. T. Perron, S. J. Martel, and K. Singha (2015), Topographic stress and rock fracture: a two-dimensional numerical model for arbitrary topography and preliminary comparison with borehole observations, Earth Surface Processes and Landforms, 40(4), 512-529.

Smith, A. P. (1972), Butteressing of Tropical Trees: A Descriptive Model and New Hypotheses, The American Naturalist, 106(947), 32-46.

1639 Smith, L. A., D. M. Eissenstat, and M. W. Kaye (2017), Variability in aboveground carbon driven by slope aspect and
1640 curvature in an eastern deciduous forest, USA, Canadian Journal of Forest Research, 47(2), 149-158,
1641 dx.doi.org/10.1139/cjfr-2016-0147.

1642 St. Clair, J., S. Moon, W. S. Holbrook, J. T. Perron, C. S. Riebe, S. J. Martel, B. Carr, C. Harman, K. Singha, and D. d.
1643 Richter (2015), Geophysical imaging reveals topographic stress control of bedrock weathering, Science, 350(6260),
1644 534-538, doi: 10.1126/science.aab2210.

1645 Staudinger, M., M. Stoelzle, S. Seeger, J. Seibert, M. Weiler, and K. Stahl (2017), Catchment water storage variation
1646 with elevation, Hydrological Processes, 31(11), 2000-2015.

1647 Steffen, W., et al. (2018), Trajectories of the Earth System in the Anthropocene, Proceedings of the National
1648 Academy of Sciences, 115 (33) 8252-8259, doi: 10.1073/pnas.1810141115.

1649 Stober, I. (2011), Depth- and pressure-dependent permeability in the upper continental crust: data from the Urach
1650 3 geothermal borehole, southwest Germany, Hydrogeology Journal, 19(3), 685-699.

1651 Stone, E. L., and P. J. Kalisz (1991), On the maximum extent of tree roots, Forest Ecology and Management, 46(1),
1652 59-102.

1653 Stringer Christina E., K. W. K., James S. Latimer (2016), Headwaters to estuaries: advances in watershed science
1654 and management - Proceedings of the Fifth Interagency Conference on Research in the Watersheds, March 2-5,
1655 2015, North Charleston, South Carolina. e-Gen. Tech. Rep. SRS-211. Asheville, NC: U.S. Department of Agriculture
1656 Forest Service, Southern Research Station, 302 p.

1657 Subin, Z. M., P. C. D. Milly, B. N. Sulman, S. Malyshev, and E. Shevliakova (2014), Resolving terrestrial ecosystem
1658 processes along a subgrid topographic gradient for an earth-system model, Hydrology and Earth System Sciences,
1659 11, 8443-8492, doi:10.5194/hessd-11-8443-2014.

1660 Sullivan, P., R. Price, M. Ross, S. Stoffella, J. Sah, L. Scinto, E. Cline, T. Dreschel, and F. Sklar (2016), Trees: a
1661 powerful geomorphic agent governing the landscape evolution of a subtropical wetland, Biogeochemistry. DOI:
1662 10.1007/s10533-016-0213-9.

1663 Swetnam, T. L., P. D. Brooks, H. R. Barnard, A. A. Harpold, and E. L. Gallo (2017), Topographically driven differences
1664 in energy and water constrain climatic control on forest carbon sequestration, Ecosphere, 8(4), e01797, doi:
1665 10.1002/ecs2.1797.

1666 Tai, X., D. S. Mackay, W. R. L. Anderegg, J. S. Sperry, and P. D. Brooks (2017), Plant hydraulics improves and
1667 topography mediates prediction of aspen mortality in southwestern USA, New Phytologist, 213(1), 113-127, doi:
1668 10.111/nph.14098.

1669 Terborgh, J (1992) Diversity and the Tropical Rainforest (Scientific American Library, Book 38), W H Freeman & Co.,
1670 242 pages.

1671 Tesfa, T. K., D. G. Tarboton, D. G. Chandler, and J. P. McNamara (2009), Modeling soil depth from topographic and
1672 land cover attributes, Water Resources Research, 45(10), W10438, doi: 10.1029/2008WR007474.

1673 Thompson J, J. P., V Viana, J A Ratter, and D A Scott (1992), The forest-savanna boundary o Maraca Island,
1674 Roraima, Brazil: An investigation of two contrasting transects, in Nature and Dynamics of Forest-Savanna
1675 Boundaries (ed Furley PA, J Proctor, and J A Ratter), Chapman & Hall, Suffolk, UK 616 pages.

1676 Tomasella, J., M. G. Hodnett, and L. Rossato (2000), Pedotransfer function for the estimation of soil water
1677 retention in Brazilian soils, Soil Sci. Soc. Am. J., 64, 327–338, doi:10.2136/sssaj2000.641327x.

1678 Tóth, J. (1963), A theoretical analysis of groundwater flow in small drainage basins, Journal of Geophysical
1679 Research, 68(16), 4795-4812.

1680 Troch, P. A., C. Paniconi, and E. Emiel van Loon (2003), Hillslope-storage Boussinesq model for subsurface flow and
1681 variable source areas along complex hillslopes: 1. Formulation and characteristic response, Water Resources
1682 Research, 39(11), 1316, doi:10.1029/2002wr001728.

1683 Turc, L. (1954), Le bilan d'eau des sols: relation entre la precipitations, l'evaporation et l'ecoulement,
1684 Annales Agronomiques, Serie A(5), 491 – 569.

1685 Verdin, K.L. (2017), Hydrologic Derivatives for Modeling and Applications (HDMA) database: U.S. Geological Survey
1686 data release, https://doi.org/10.5066/F7S180ZP. Data available at
1687 https://www.sciencebase.gov/catalog/item/5910def6e4b0e541a03ac98c

1688 Villalobos-Vega, R. (2010), Water table and nutrient dynamics in neotropical savannas and wetland ecosystems,
1689 Electronic dissertation 389. University of Miami, [http://scholarlyrepository.miami.edu/oa_dissertations/389.].

1690 Vrettas, M. D., and I. Y. Fung (2015), Toward a new parameterization of hydraulic conductivity in climate models:
1691 Simulation of rapid groundwater fluctuations in Northern California, Journal of Advances in Modeling Earth
1692 Systems, 7(4), 2105-2135, doi:10.1002/2015MS000516.

1693 Vrettas, M. D., and I. Y. Fung (2017), Sensitivity of transpiration to subsurface properties: Exploration with a 1-D
1694 model, Journal of Advances in Modeling Earth Systems, 9(2), 1030-1045, doi:10.1002/ 2016MS000901.

1695 Wagener, T., M. Sivapalan, P. Troch, and R. Woods (2007), Catchment Classification and Hydrologic Similarity,
1696 Geography Compass, 1(4), 901-931, doi:10.1111/j.1749-8198.2007.00039.x.

1697 Wagener, T., M. Sivapalan, P. A. Troch, B. L. McGlynn, C. J. Harman, H. V. Gupta, P. Kumar, P. S. C. Rao, N. B. Basu,
1698 and J. S. Wilson (2010), The future of hydrology: An evolving science for a changing world, Water Resources
1699 Research, 46(5), W05301, doi:10.1029/2009WR008906.

1700 Walko, R. L., L.E. Band, J. S. Baron, T. G. F. Kittel, R. Lammers, T. J. Lee, D. Ojima, R. A. Pielke Sr., C. Taylor, C. Tague,
1701 C. J. Tremback, and P. L. Vidale (2000), Coupled Atmosphere–Biophysics–Hydrology Models for Environmental
1702 Modeling, Journal of Applied Meteorology, 39(6), 931-944.

1703 Wang, X.-S., X.-W. Jiang, L. Wan, S. Ge, and H. Li (2011), A new analytical solution of topography-driven flow in a
1704 drainage basin with depth-dependent anisotropy of permeability, Water Resources Research, 47(9), W09603,
1705 doi:10.1029/2011WR010507.

1706 Wang-Erlandsson, L., W. G. Bastiaanssen, H. Gao, J. Jägermeyr, G. B. Senay, A. I. Van Dijk, J. P. Guerschman, P. W.
1707 Keys, L. J. Gordon, and H. H. Savenije (2016), Global root zone storage capacity from satellite-based evaporation,
1708 Hydrology and Earth System Sciences, 20(4), 1459-1481, http://dx.doi.org/10.5194/hess- 20- 1459- 2016.

1709 Weaver, J. E. (1919), The Ecological Relations of Roots. Digital Commons @ University of Nebraska-Lincoln, 122-
1710 127.

1711 Webb, R. S., C. E. Rosenzweig, and E. R. Levine (1993), Specifying land surface characteristics in general circulation
1712 models: Soil profile data set and derived water-holding capacities, Global Biogeochemical Cycles, 7(1), 97-108.

1713 Weeks, J. B., E. D. Gutentag, F. J. Heimes, and R. R. Luckey (1988), Summary of the high plains regional aquifer-
1714 system analysis in parts of Colorado, Kansas, Nebraska, New Mexico, Oklahoma, South Dakota, Texas, and
1715 Wyoming, US Geological Survey professional paper (USA), 1400-A, 30 pp.

1716 Weintraub, S. R., Brooks, P. D. & Bowen (2017), Interactive Effects of Vegetation Type and Topographic Position on
1717 Nitrogen Availability and Loss in a Temperate Montane Ecosystem, J. Ecosystems, 20(6), 1073–1088.

1718 Whittaker, R. H. (1956), Vegetation of the Great Smoky Mountains, Ecological Monographs, 26(1), 1-80.

1719 Wilson, C., and W. E. Dietrich (1987), The contribution of bedrock groundwater flow to storm runoff and high pore
1720 water pressure development in hollows, Proc. Int. Symp. on Erosion and Sedimentation in the Pacific Rim, 3-7
1721 August 1987, Corvallis, Ore., Int. Assoc. Hydrological Sciences Bull., IAHS Publ., 165, 49-59.

1722 Winter, T. C., J. W. Harvey, O. L. Franke, and W. A. Alley (1998), Ground water and surface water: A single resource,
1723 U.S. Geol. Surv. Circ., 1139, 79 pp.

1724 Worthington, S. R. H., G. J. Davies, and E. C. Alexander (2016), Enhancement of bedrock permeability by
1725 weathering, Earth-Science Reviews, 160, 188-202, https://doi.org/10.1016/j.earscirev.2016.07.002.

1726 Xu, X., and W. Liu (2017), The global distribution of Earth's critical zone and its controlling factors, Geophysical
1727 Research Letters, 44(7), 3201-3208, doi:10.1002/2017GL072760.

1728 Yamazaki, D., T. Oki, and S. Kanae (2009), Deriving a global river network map and its sub-grid topographic
1729 characteristics from a fine-resolution flow direction map, Hydrology and Earth System Sciences, 13(11), 2241,
1730 Retrieved from https://search.proquest.com/docview/907230425?accountid=13626.

Yamazaki, D., S. Kanae, H. Kim, and T. Oki (2011), A physically based description of floodplain inundation dynamics in a global river routing model, Water Resources Research, 47(4), W04501, doi:10.1029/2010WR009726.

Yamazaki, D., D. Ikeshima, R. Tawatari, T. Yamaguchi, F. O'Loughlin, J. C. Neal, C. C. Sampson, S. Kanae, and P. D. Bates (2017), A high-accuracy map of global terrain elevations, Geophysical Research Letters, 44(11), 5844-5853, doi: 10.1002/2017GL072874.

Yang, Y., R. J. Donohue, and T. R. McVicar (2016), Global estimation of effective plant rooting depth: Implications for hydrological modeling, Water Resources Research, 52(10), 8260-8276, doi:10.1002/2016WR019392.

Zapata-Rios, X., P. D. Brooks, P. A. Troch, J. McIntosh, and Q. Guo (2016), Influence of terrain aspect on water partitioning, vegetation structure and vegetation greening in high-elevation catchments in northern New Mexico, Ecohydrology, 9(5), 782-795, https://doi.org/10.1002/eco.1674.

Zhang, Z., N. E. Zimmermann, J. O. Kaplan, and B. Poulter (2016), Modeling spatiotemporal dynamics of global wetlands: comprehensive evaluation of a new sub-grid TOPMODEL parameterization and uncertainties, Biogeosciences, 13(5), 1387-1408, doi: 10.5194/bg-13-1387-2016.

Zheng, X., D. G. Tarboton, D. R. Maidment, Y. Y. Liu, and P. Passalacqua (2018), River Channel Geometry and Rating Curve Estimation Using Height above the Nearest Drainage, JAWRA Journal of the American Water Resources Association, 54(4), 785-806, http://doi.org/10.1111/1752-1688.12661.

Figure 1.

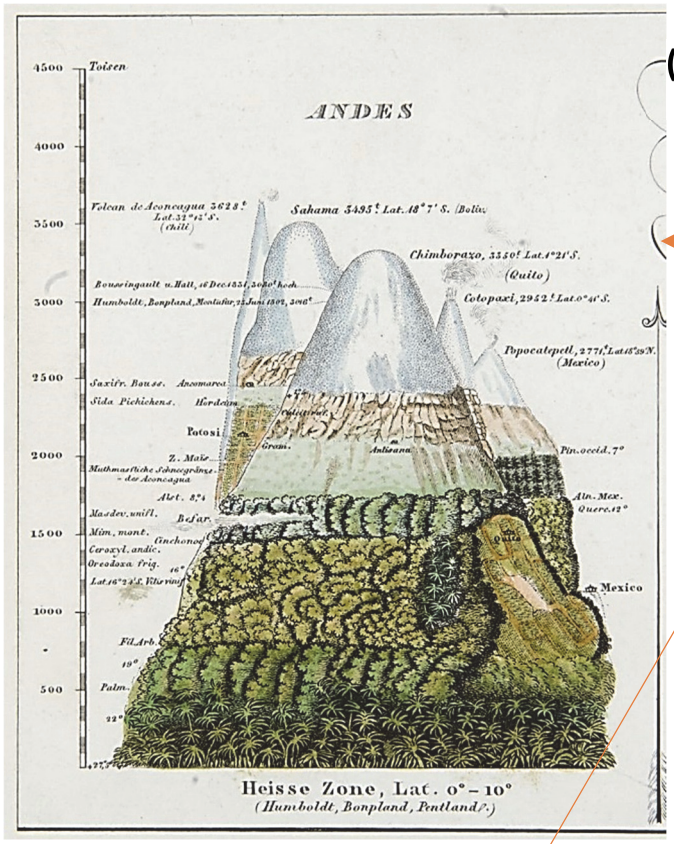
ANDES
Toisen
4500
4000
3500
3000
2500
2000
1500
1000
500
Volcan de Aconcagua 3628 t. Lat. 32°72' S. (chili)
Sahama 3495 t. Lat. 18°7' S. (Bolivia)
Chimborazo, 3350t Lat. 1°21' S. (Quito)
Cotopaxi, 2952 t. Lat. 0°41' S.
Popocatepell, 2771t. Lat. 19°2' N. (Mexico)
Humboldt, Bonpland, Montufar, 22 Jan. 1803, 20,000'
Saxifr. Bauze. Ancomarca
Sida Pichichens. Hordeum
Cultivated
Potosi
Gram.
Antisana
Pin. occid. 7°
Z. Mais
Mathmatische Schneegränze - der Aconcagua
Alt. 8°1
Aln. Mex.
Quere. 12°
Masdev. unifl. Befar.
Mim. mont. (Cinchona)
Cerozyl. andic.
Oreodoxa frig. 16°
Lat. 16°2 1/2' Vitoria
Mexico
Fil. Arb.
19°
Palm.
22°
Heisse Zone, Lat. 0° – 10°
(Humboldt, Bonpland, Pentland &c.)

(b)

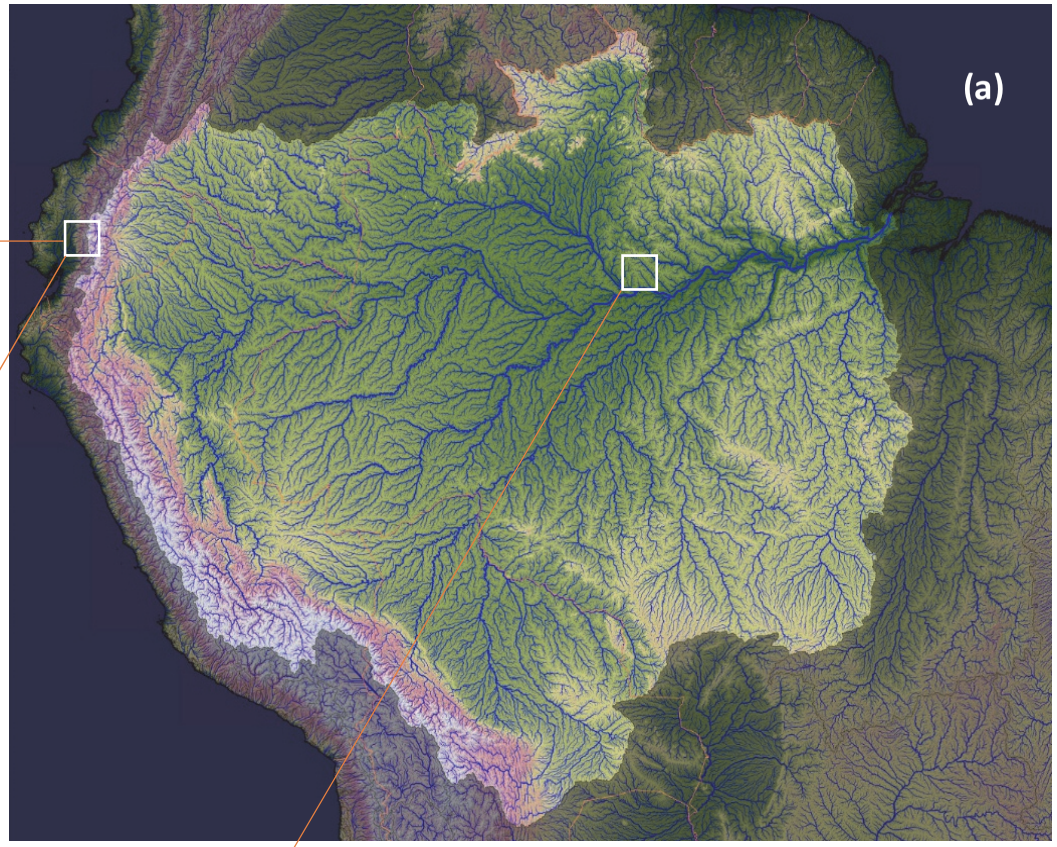
(a)

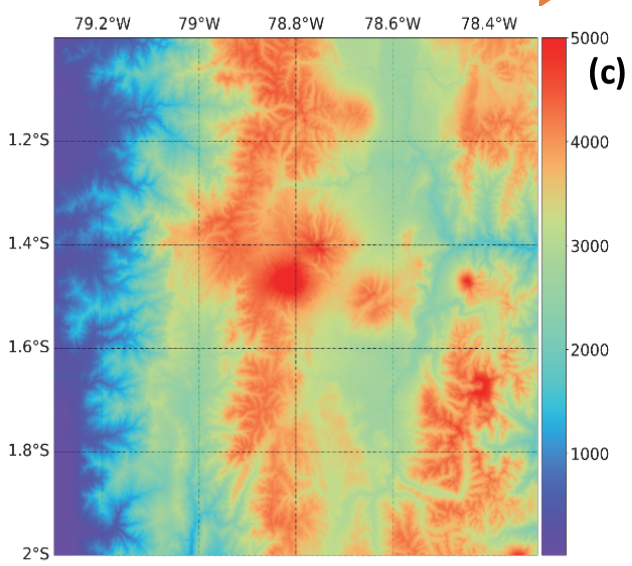
79.2°W
79°W
78.8°W
78.6°W
78.4°W
1.2°S
1.4°S
1.6°S
1.8°S
2°S
5000
4000
3000
2000
1000
(c)

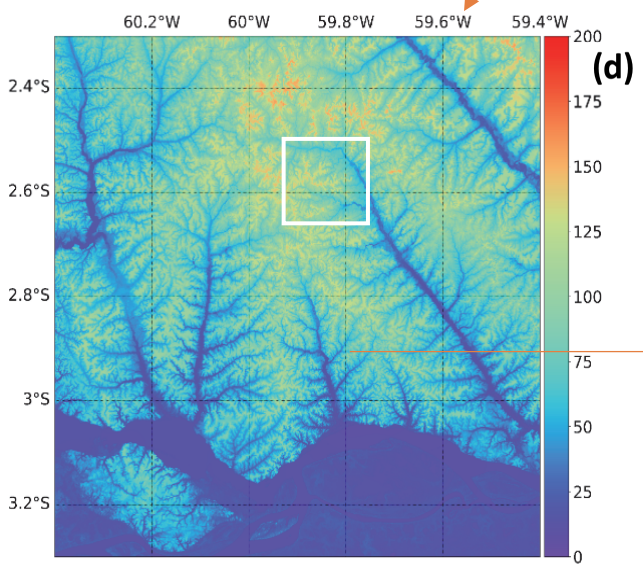
60.2°W
60°W
59.8°W
59.6°W
59.4°W
2.4°S
2.6°S
2.8°S
3°S
3.2°S
200
175
150
125
100
75
50
25
0
(d)

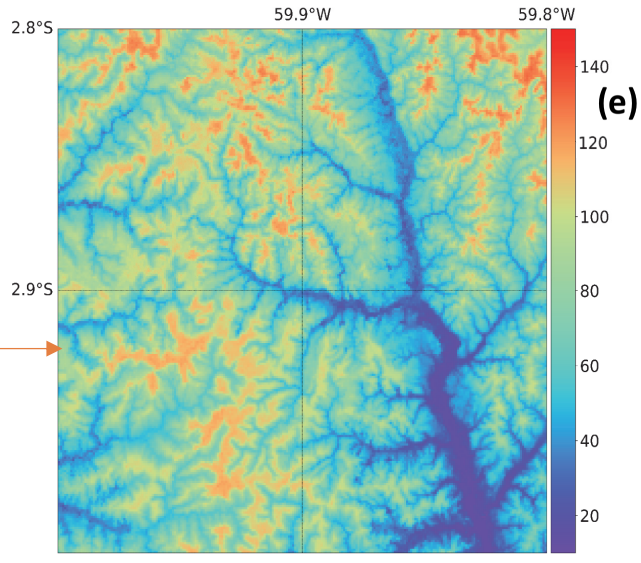
59.9°W
59.8°W
2.8°S
2.9°S
140
120
100
80
60
40
20
(e)

Figure 2.

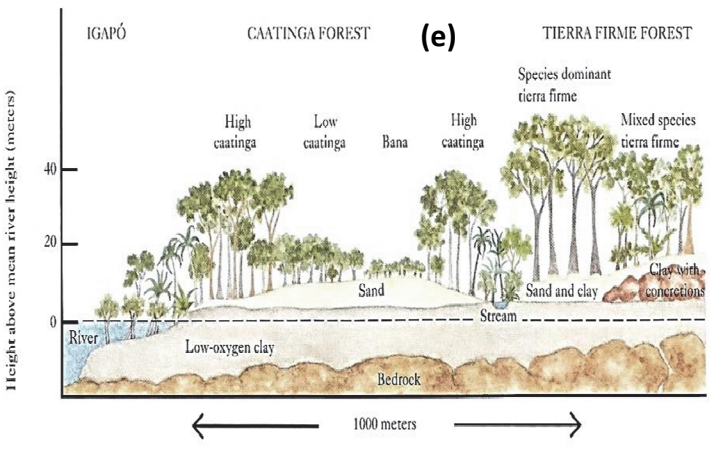

A schematic cross section of the varied terrain near San Carlos del Rio Negro, Venezuela, showing how dramatically the vegetation responds to small differences in soil type and elevation above the water table.

Figure 3.


(a)


(b)
Google earth

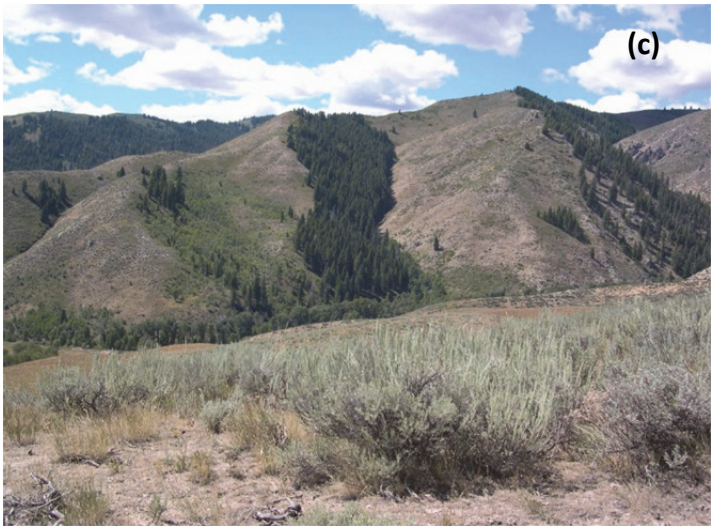
(c)


(d)


(e)


(f)
Google Earth

Figure 4.

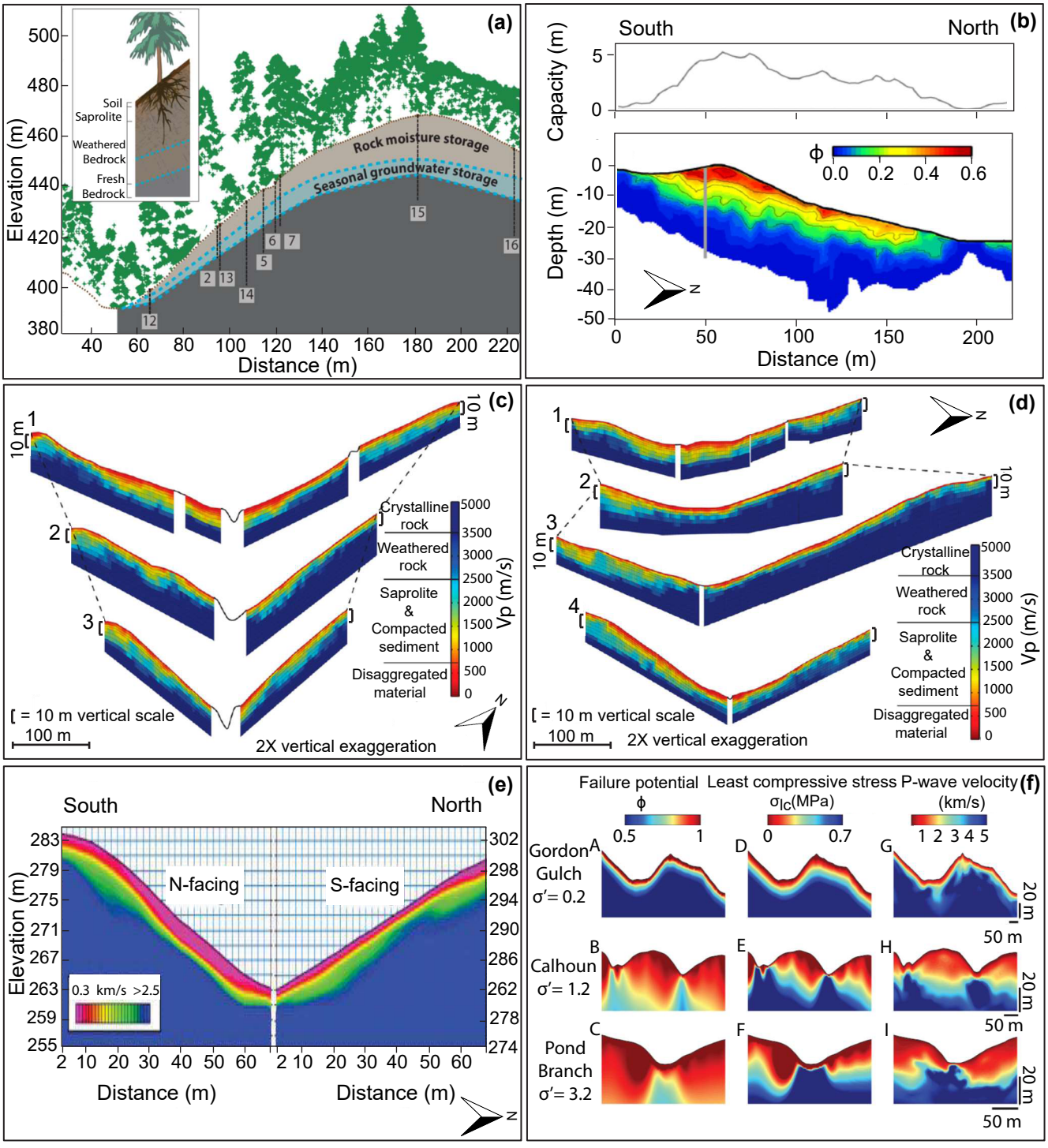
(a)
Elevation (m)
Distance (m)
Soil
Saprolite
Weathered Bedrock
Fresh Bedrock
Rock moisture storage
Seasonal groundwater storage
(b)
South
North
Capacity (m)
Depth (m)
Distance (m)
ϕ
0.0 0.2 0.4 0.6
(c)
10 m
Crystalline rock
Weathered rock
Saprolite & Compacted sediment
Disaggregated material
Vp (m/s)
[= 10 m vertical scale
100 m
2X vertical exaggeration
(d)
Vp (m/s)
[= 10 m vertical scale
100 m
2X vertical exaggeration
(e)
South
North
N-facing
S-facing
Elevation (m)
0.3 km/s >2.5
Distance (m)
(f)
Failure potential
Least compressive stress
P-wave velocity
ϕ
σlc(MPa)
(km/s)
Gordon Gulch σ′= 0.2
Calhoun σ′= 1.2
Pond Branch σ′= 3.2
20 m
50 m

Figure 5.

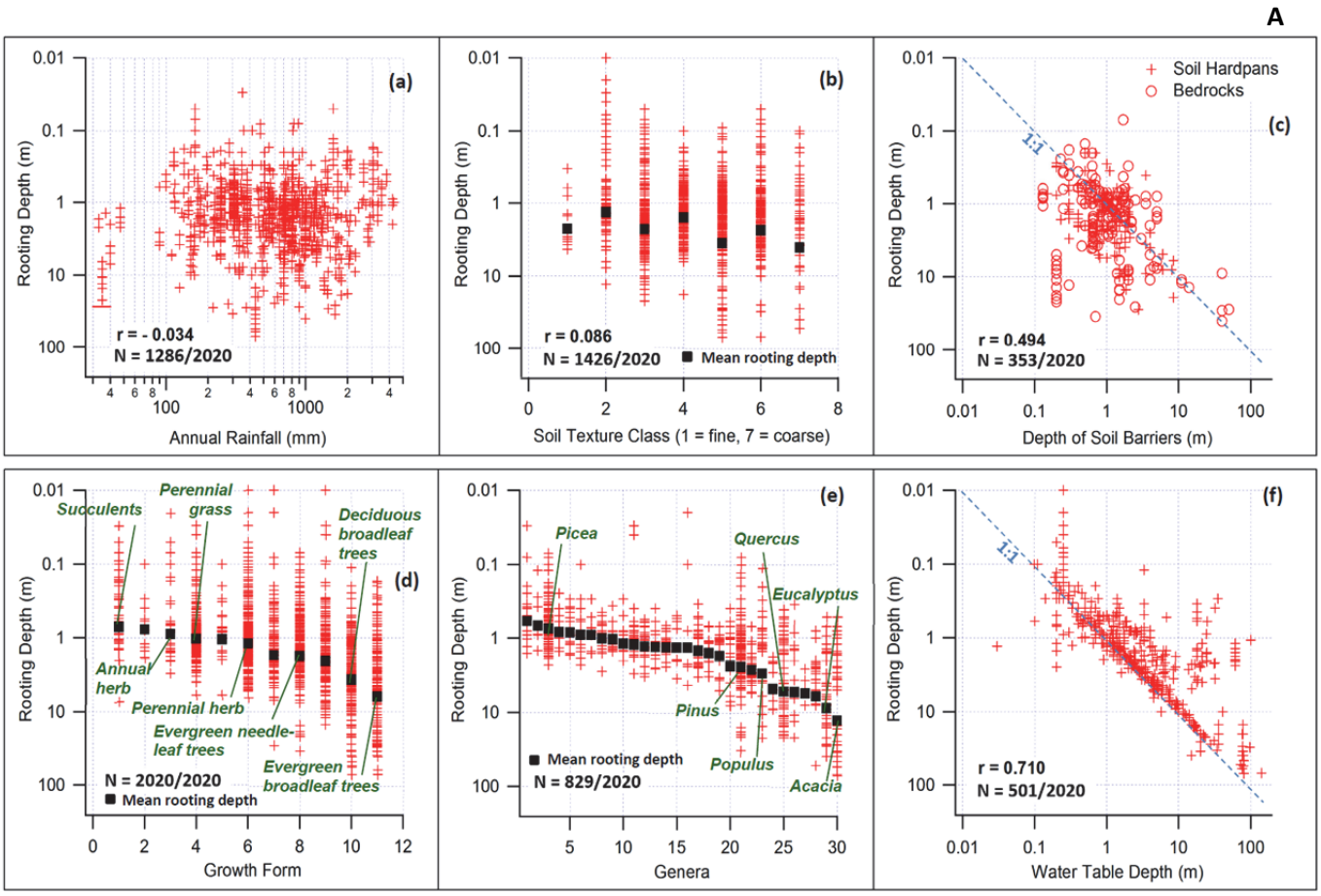
A
(a)
Rooting Depth (m)
r = - 0.034
N = 1286/2020
Annual Rainfall (mm)
(b)
r = 0.086
N = 1426/2020
Mean rooting depth
Soil Texture Class (1 = fine, 7 = coarse)
(c)
Soil Hardpans
Bedrocks
1:1
r = 0.494
N = 353/2020
Depth of Soil Barriers (m)
(d)
Succulents
Perennial grass
Deciduous broadleaf trees
Annual herb
Perennial herb
Evergreen needle-leaf trees
Evergreen broadleaf trees
N = 2020/2020
Mean rooting depth
Growth Form
(e)
Picea
Quercus
Eucalyptus
Pinus
Populus
Acacia
Mean rooting depth
N = 829/2020
Genera
(f)
1:1
r = 0.710
N = 501/2020
Water Table Depth (m)

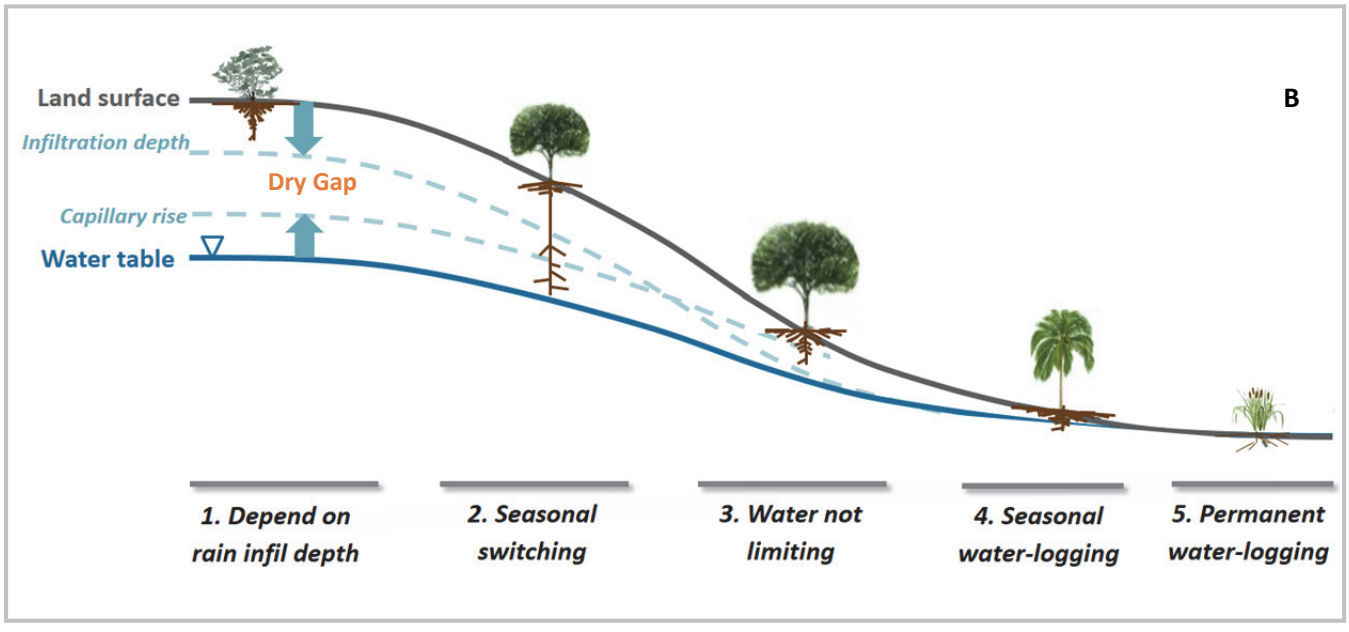
B
Land surface
Infiltration depth
Dry Gap
Capillary rise
Water table
1. Depend on rain infil depth
2. Seasonal switching
3. Water not limiting
4. Seasonal water-logging
5. Permanent water-logging

Figure 6.

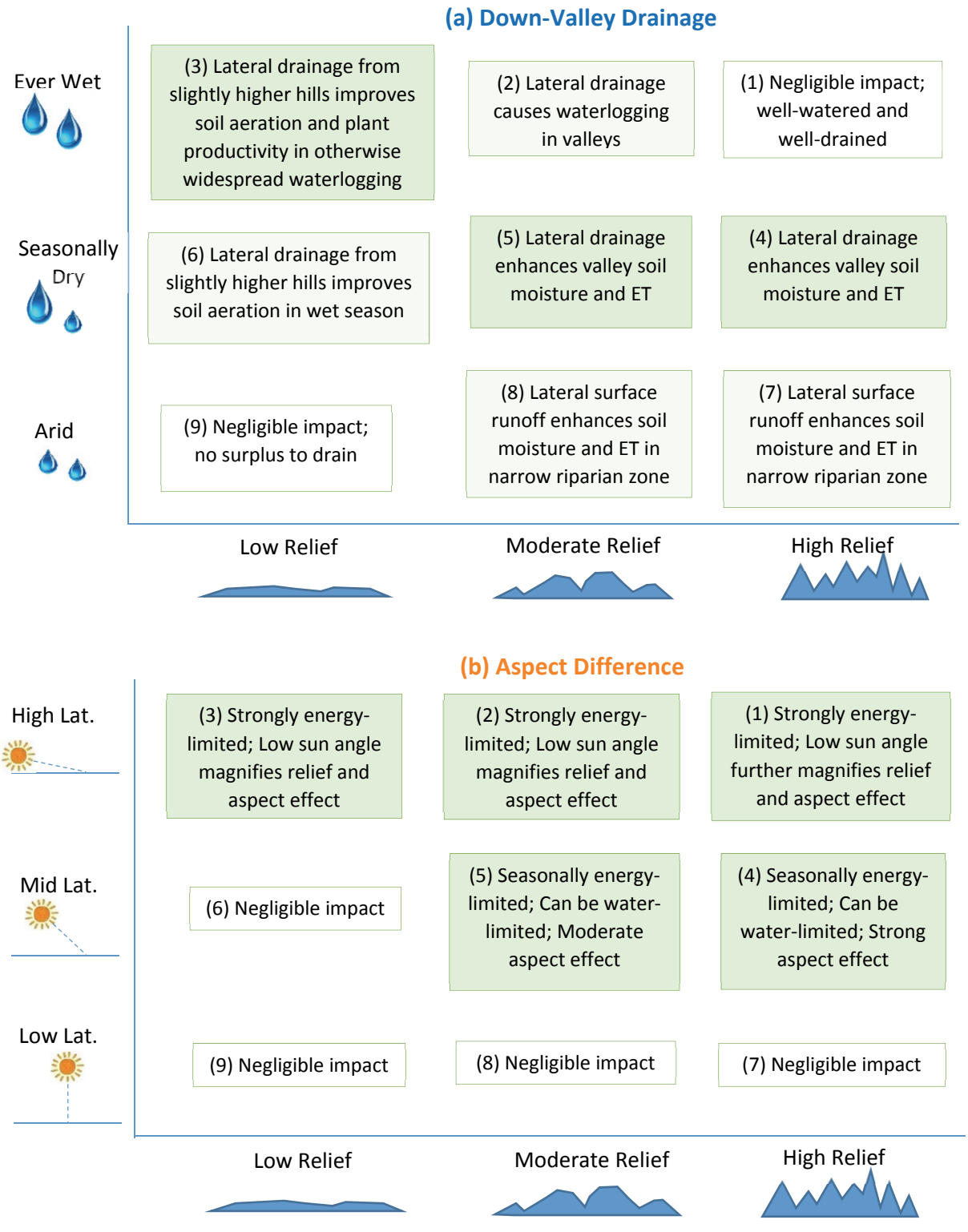
(a) Down-Valley Drainage
Ever Wet
(3) Lateral drainage from slightly higher hills improves soil aeration and plant productivity in otherwise widespread waterlogging
(2) Lateral drainage causes waterlogging in valleys
(1) Negligible impact; well-watered and well-drained
Seasonally Dry
(6) Lateral drainage from slightly higher hills improves soil aeration in wet season
(5) Lateral drainage enhances valley soil moisture and ET
(4) Lateral drainage enhances valley soil moisture and ET
Arid
(9) Negligible impact; no surplus to drain
(8) Lateral surface runoff enhances soil moisture and ET in narrow riparian zone
(7) Lateral surface runoff enhances soil moisture and ET in narrow riparian zone
Low Relief
Moderate Relief
High Relief
(b) Aspect Difference
High Lat.
(3) Strongly energy-limited; Low sun angle magnifies relief and aspect effect
(2) Strongly energy-limited; Low sun angle magnifies relief and aspect effect
(1) Strongly energy-limited; Low sun angle further magnifies relief and aspect effect
Mid Lat.
(6) Negligible impact
(5) Seasonally energy-limited; Can be water-limited; Moderate aspect effect
(4) Seasonally energy-limited; Can be water-limited; Strong aspect effect
Low Lat.
(9) Negligible impact
(8) Negligible impact
(7) Negligible impact
Low Relief
Moderate Relief
High Relief

Figure 7.

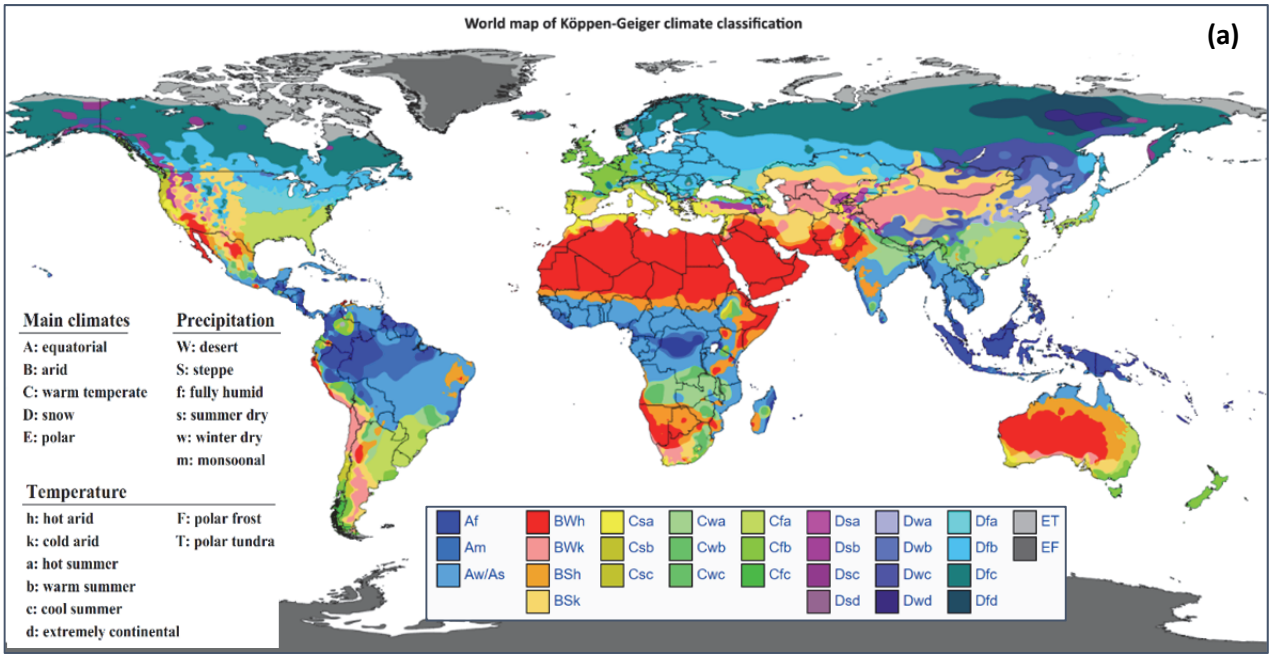

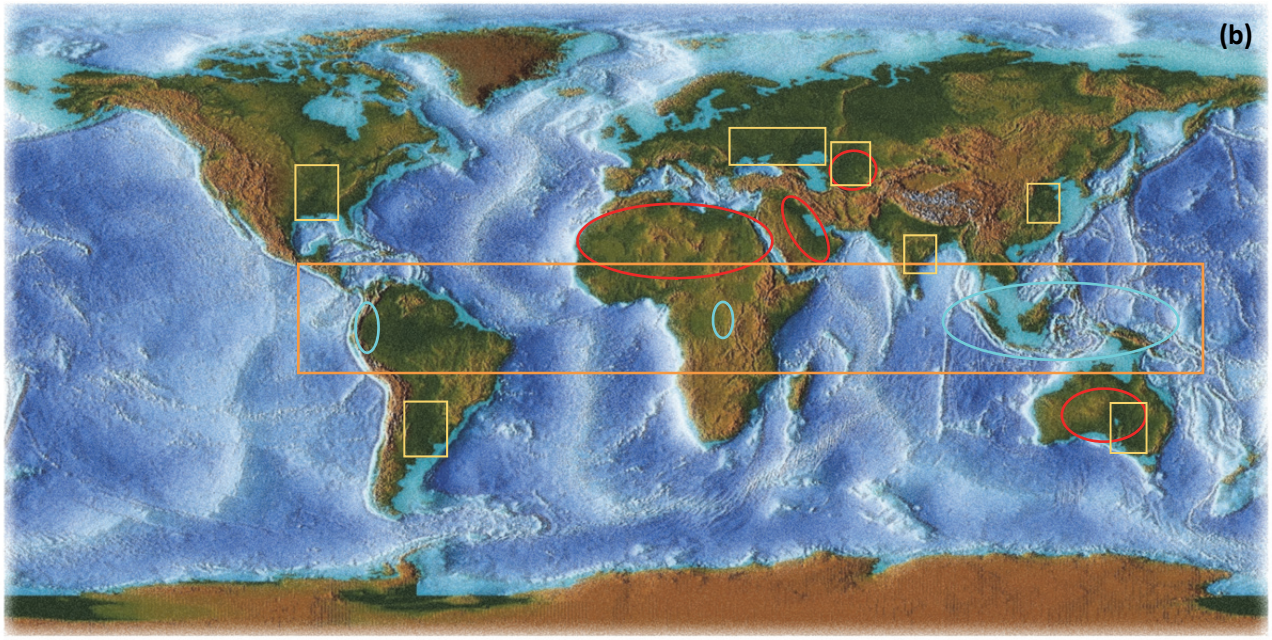

Drainage ○ Position-1: ever-wet (Af), high-relief ○ Position-9: arid (Bwh, Bwk), low-relief

Aspect □ Position-7, 8, 9: low-latitude, all relief □ Position-6: mid latitude, low-relief

Figure 8.

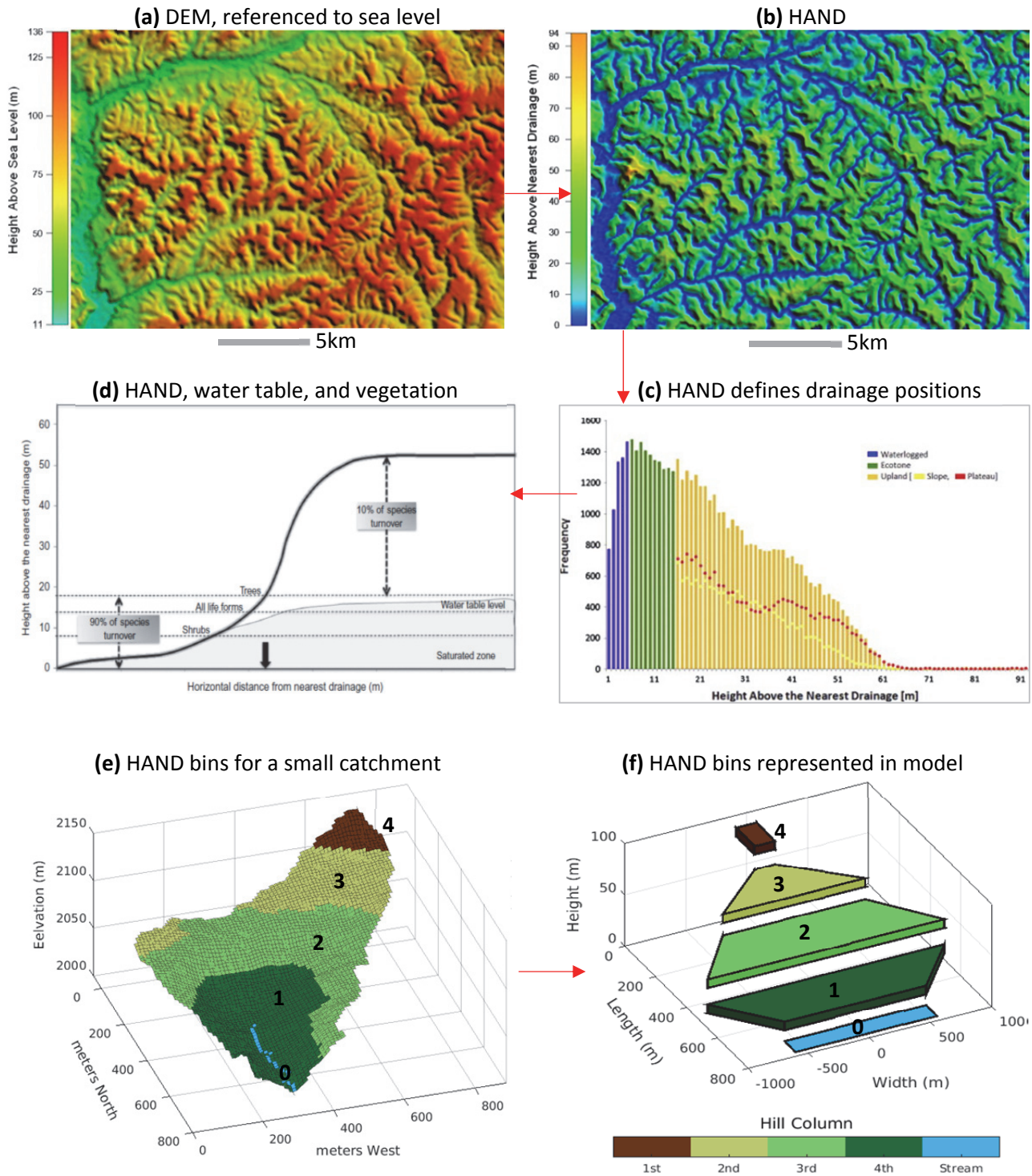
(a) DEM, referenced to sea level
Height Above Sea Level (m)
136
125
100
75
50
25
11
5km
(b) HAND
Height Above Nearest Drainage (m)
94
90
80
70
60
50
40
30
20
10
0
5km
(d) HAND, water table, and vegetation
Height above the nearest drainage (m)
60
50
40
30
20
10
0
10% of species turnover
Trees
All life forms
Water table level
90% of species turnover
Shrubs
Saturated zone
Horizontal distance from nearest drainage (m)
(c) HAND defines drainage positions
Frequency
1600
1400
1200
1000
800
600
400
200
0
Waterlogged
Ecotone
Upland [
Slope,
Plateau]
1
11
21
31
41
51
61
71
81
91
Height Above the Nearest Drainage [m]
(e) HAND bins for a small catchment
Eelvation (m)
2150
2100
2050
2000
4
3
2
1
0
0
200
400
600
800
meters North
0
200
400
600
800
meters West
(f) HAND bins represented in model
Height (m)
100
50
0
4
3
2
1
0
0
200
400
600
800
Length (m)
-1000
-500
0
500
100
Width (m)
Hill Column
1st
2nd
3rd
4th
Stream

Figure 9.

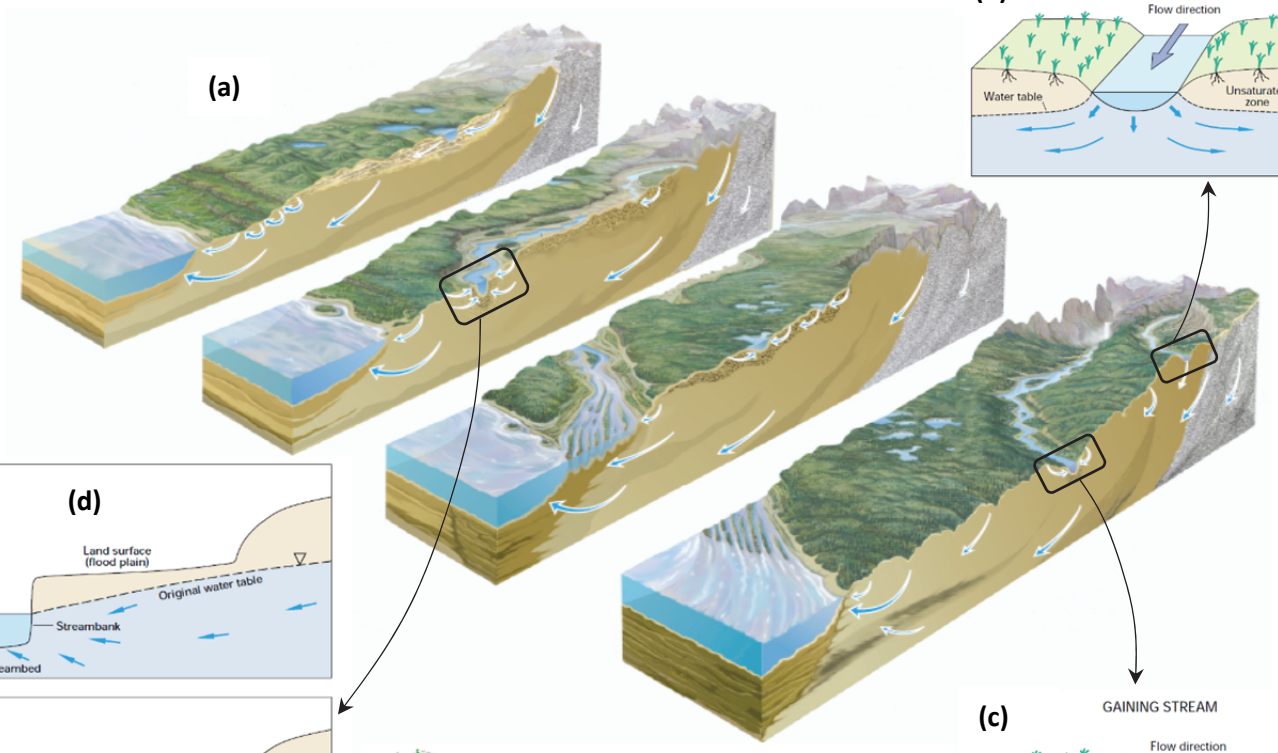
(a)
(b)
LOSING STREAM
Flow direction
Water table
Unsaturated zone
(c)
GAINING STREAM
Flow direction
Unsaturated zone
Water table
Shallow aquifer

A
(d)
Land surface (flood plain)
Original water table
Streambank
Streambed

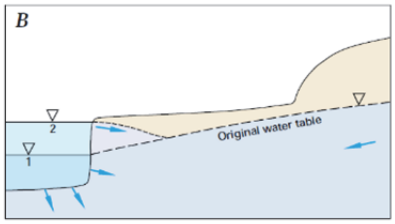
B
Original water table

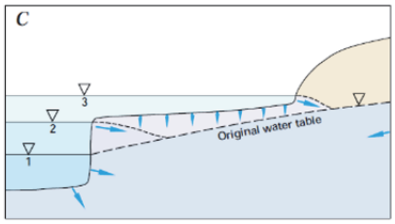
C
Original water table

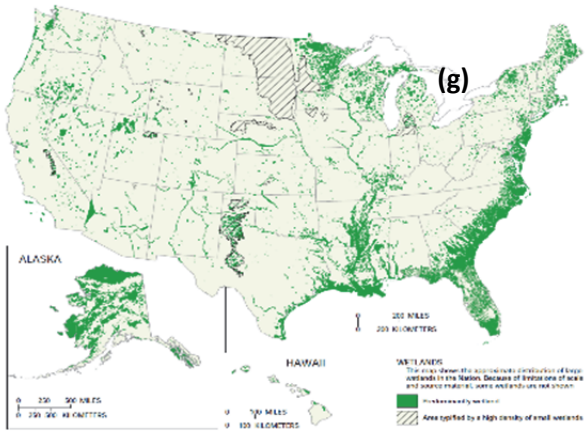
(g)
ALASKA
HAWAII
WETLANDS

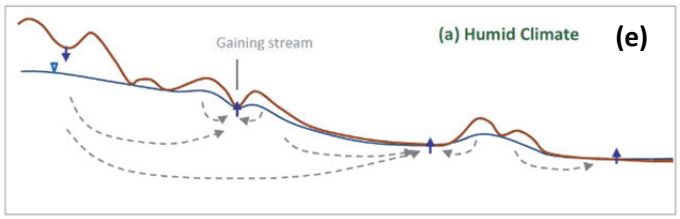
Gaining stream
(a) Humid Climate
(e)

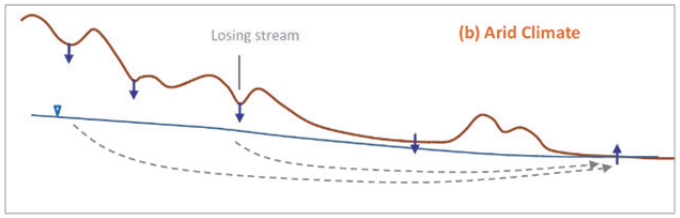
Losing stream
(b) Arid Climate

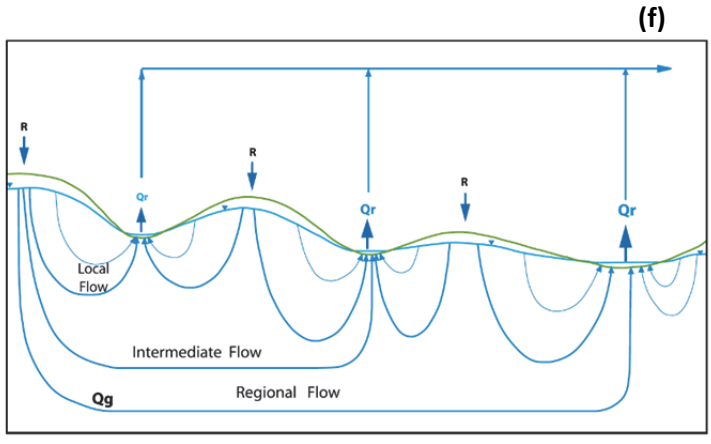
(f)
R
Qr
Local Flow
Intermediate Flow
Qg
Regional Flow